THE JOURNAL OF PHYSICAL CHEMISTRY A

Article

pubs.acs.org/JPCA

Reaction Path Bifurcation in an Electrocyclic Reaction: Ring-Opening of the Cyclopropyl Radical

Zeb C. Kramer,*[,†] Barry K. Carpenter,*[,‡] Gregory S. Ezra,*[,†] and Stephen Wiggins*[,§]

[†]Department of Chemistry and Chemical Biology, Cornell University, Baker Laboratory, Ithaca, New York 14853 United States

[‡]School of Chemistry, University of Cardiff, Cardiff CF10 3AT, United Kingdom

[§]School of Mathematics, University of Bristol, Bristol BS8 1TW, United Kingdom

Supporting Information

ABSTRACT: Following previous work [*J. Chem. Phys.* **2013**, *139*, 154108] on a simple model of a reaction with a post-transition state valley ridge inflection point, we study the chemically important example of the electrocyclic cyclopropyl radical ring-opening reaction using direct dynamics and a reduced dimensional potential energy surface. The overall reaction requires con- or disrotation of the methylenes, but the initial stage of the ring-opening involves substantial internal rotation of only one methylene. The reaction path bifurcation is then associated with the relative sense of rotation of the second methylene. Clear deviations of reactive trajectories from the disrotatory intrinsic reaction coordinate (IRC) for the ring-opening are observed and the dynamical mechanism is discussed. Several features observed in the model system are found to be preserved in the more complex and higher dimensional ring-opening reaction. Most notable is the sensitivity of the reaction mechanism to the shape of the potential manifested as a Newtonian kinetic isotope effect upon deuterium substitution of one of the methylene hydrogens. Dependence of the product yield on frictional dissipation representing external environmental effects is also presented. The dynamics of the post-transition state cyclopropyl radical ring-opening are discussed in detail, and the use of low dimensional models as tools to analyze complicated organic reaction mechanisms is assessed in the context of this reaction.

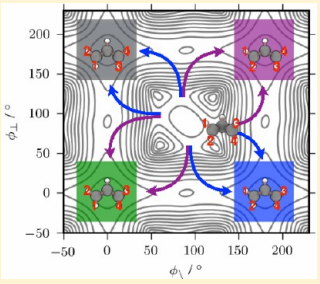

INTRODUCTION

The thermal electrocyclic ring-opening of the cyclopropyl radical to form the allyl radical exemplifies the difficulty of obtaining accurate mechanistic descriptions of even relatively simple organic reactions. Interest focused on this particular system during the development of the Woodward−Hoffmann rules.[1] These rules predicted a synchronous *conrotatory* mechanism, where the planes of the two terminal CH_2 groups of the molecule rotated in the same direction into the three-carbon (3C) plane.[2] Contrary to this prediction, the orbital correlation diagram approach of Abrahamson and Longuet-Higgins showed that the symmetry-preserving, synchronous mechanisms (symmetry group C_2 for conrotatory opening and C_s for disrotatory opening) correlated the ground state of the cyclopropyl radical to excited states of the allyl radical product[3] when more orbitals than just the highest energy frontier orbital were considered. This result implied that the electronically adiabatic reaction on the ground state is symmetry forbidden. As Szeimies and Boche note,[4] the experimentally measured activation energy of approximately 22 kcal mol^{-1} [5−7] is somewhat lower than expected for the generation of a electronically excited product. This discrepancy was resolved by the semiempirical MNDO calculations of Dewar and Kirschner[8] (confirmed using more rigorous *ab initio* methods[9−13]), which showed that the transition state (TS) of the ring-opening is not symmetric but rather has one CH_2 group forming a ∼60° dihedral angle with the 3C plane while the other CH_2 is nearly perpendicular to the 3C plane, Figure 1. Henceforth, these two CH_2 groups are denoted *tilt*-CH_2 and *perp*-CH_2, respectively.

Relaxing the symmetry requirement on the TS reveals that the ring-opening may favor a reaction path on the ground state electronic potential energy surface (PES) where the two CH_2 groups rotate into the 3C plane in an asynchronous fashion,

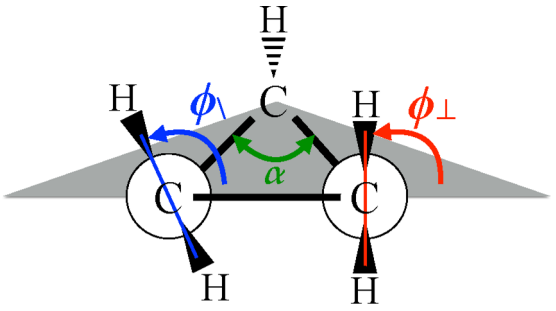

Figure 1. Important coordinates $\phi_\backslash$, $\phi_\perp$, and α in the ring-opening reaction are shown inset in the relevant TS structure. To be clear, the ϕ torsion angles are defined as the dihedral angles between the corresponding CH_2 planes and the three-carbon plane and the α angle is the bond angle between the two unbroken C−C bonds. At the CASSCF(3,3)/6-31+G(d,p) TS, $\phi_\backslash$ = 117° and $\phi_\perp$ = 84°.

Received: March 24, 2015
Revised: June 3, 2015
Published: June 3, 2015

DOI: 10.1021/acs.jpca.5b02834
J. Phys. Chem. A 2015, 119, 6611−6630

thereby breaking the symmetry and lowering the reaction energy barrier.[4,10] Calculations of the intrinsic reaction coordinate (IRC)[14] imply a mechanism where the *tilt*-CH_2 rotates significantly as the carbon backbone opens before the *perp*-CH_2 rotates *disrotatorily* into the 3C plane.[9−11]

Although the IRC is clearly disrotatory, two features of this reaction path allow for the possibility of a significant dependence of the mechanism on the dynamics past the TS. First, the energy difference between the TS and the allyl product is relatively large, ∼55 kcal mol^{-1}. It is found that a large amount of potential energy is transferred to kinetic energy (KE) of a small number of degrees of freedom, including the CH_2 rotations and the bond angle of the opening ring. Second, much of the steep drop in the potential occurs prior to the rotation of *perp*-CH_2 on the IRC, so that the remainder of the IRC, consisting primarily of the *perp*-CH_2 rotation, traverses a region of the PES that is a relatively low energy ridge prior to reaching the allyl product. In this region of the PES, with the kinetic energy imparted during the descent from the high barrier, the system need not follow the IRC, and the *perp*-CH_2 can complete its rotation into the allyl product well via either dis- or conrotatory rotations.

Quapp and co-workers have established the existence of a post-TS valley ridge inflection (VRI) point,[15,16] where the PES undergoes a transition from a valley-like structure near the first-order saddle point of the TS to a ridge-like structure separating the two allyl product wells. The presence of this VRI point suggests the ring-opening process contains a reaction path bifurcation,[15−25] which further confounds any mechanistic predictions based solely on the PES topography. Therefore, the details of the dynamics past the TS are of critical importance to an understanding of the ring-opening mechanism, and the cyclopropyl ring-opening cannot be simplistically reduced to a 1d picture of progress along a reaction path.[26] In particular, momenta associated with the "active" degrees of freedom of the reaction play a central part in the ring-opening mechanism.

The first direct dynamics study of the cyclopropyl radical ring-opening was performed by Mann and Hase[27] using "on-the-fly" gradients. In their work, cyclopropyl ring-opening trajectories were initiated on the transition state dividing surface associated with the TS (index 1 saddle) with initial conditions consistent with a temperature of 174 °C.[5,6] Under these conditions, Mann and Hase found that 57% of the reactive trajectories followed the asynchronous disrotatory mechanism whereas only 43% opened via an asynchronous conrotatory mechanism. The time interval between the initial rotations of the *perp*-CH_2 and the *tilt*-CH_2 was found to be much shorter for the conrotatory trajectories, 35 fs versus 56 fs for the disrotatory trajectories. Mann and Hase also noted that on average disrotatory trajectories were initialized at the TS with relatively higher energy in the reaction coordinate. All reactive trajectories were found to be asynchronous and ∼50% of the reacting trajectories went on to undergo subsequent rotations of the CH_2 groups during the propagation time of 200 fs, passing between allyl product conformer wells. These subsequent rotations occurred on a time scale much faster than the 488 fs RRKM predicted time scale calculated by Mann and Hase. This suggests that the product yield of the indistinguishable stereoisomers from a given TS may be dominated by longer time dynamics where intramolecular vibrational redistribution (IVR) and/or energy dissipation restore thermal equilibrium and a thermal stereoisomer product yield.

Mann and Halls[28] considered the effects of environmental dissipation by performing direct dynamics trajectories with the cyclopropyl radical immersed in model argon and helium solvent baths at different pressures and at T = 447 K. At higher pressures, the disrotatory pathway predicted by the IRC was strongly dominant. The bath was also found to suppress further CH_2 rotations between the stereoisomers of the allyl product, with few such rotations observed at low pressure and none observed at high pressure on the 200 fs propagation time scale. This finding indicates that the time scale of interaction of the allyl product with its environment greatly influences the stereospecificity of the reaction and may provide some degree of kinetic control in this reaction. Indeed, our earlier work has suggested that a system with a bifurcating reaction path can show surprising variability in product yield in the presence of dissipation due to the competing time scales of product interconversion.[25] Further effects of dissipation on the ring-opening reaction are considered in this work.

From the discussion above, it is clear that the cyclopropyl radical ring-opening belongs to that class of organic reactions whose mechanisms cannot be simply inferred either from a small set of stationary points on the PES or from the IRC.[29−35] For many of these reactions, it is found that conventional statistical theories of reaction, namely transition state theory (TST) and RRKM,[36] fail to predict isotope effects and, often more importantly, product selectivities.[37−39] Dynamical studies of nonstatistical reactions are reshaping our fundamental conceptions of mechanistic physical organic chemistry with profound significance in areas such as synthetic organic chemistry,[38] enzyme catalysis,[40] and reactive roaming.[41,42] The ring-opening of the cyclopropyl radical is one of the simplest examples of an electrocyclic reaction and additionally contains a VRI point on its PES, characteristic of reactions with a bifurcating reaction path. The cyclopropyl radical is, therefore, of interest as a prototype of more complicated electrocyclic systems.[35]

The present study follows up on recent work[25] on a two degree of freedom (2d) model PES exhibiting a VRI point, a lower dimensional analog of the reaction studied here. Results obtained for this 2d model potential have provided insight into the characteristic dynamics of systems with post-TS reaction path bifurcations and led to new concepts concerning mechanism-determining features of the dynamics. The 2d model was formulated to represent a general class of reactions, including electrocyclic ring-opening, in which trajectories entering the post-TS region by passage over a high barrier accelerate onto a lower energy ridge connecting the (even lower energy) product wells. The relevant VRI point occurs somewhere along a path connecting the high energy TS to the ridge, but generally not along the IRC. It is tempting to identify this VRI as a product-determining decision point in the mechanism. However, the actual role of the VRI in the reaction dynamics and product selectivity is more subtle and highly system dependent. If the ridge is particularly steep, then forces directing trajectories into the product wells just after the VRI might be expected to be mechanism and selectivity determining. However, for many systems, including the ring-opening of the cyclopropyl radical, the post-TS ridge is a region where the forces acting on trajectories in the vicinity of the VRI point are *not* necessarily mechanism determining. In such systems, it is only after trajectories have passed over the ridge that they finally reach turning points at the potential "hard wall", corresponding to highly distorted molecular config-

DOI: 10.1021/acs.jpca.5b02834
J. Phys. Chem. A 2015, 119, 6611−6630

urations, and undergo a "reflection" toward the product wells. The shape of the potential hard wall at the collision point and the nature of the dynamics in the "over-the-ridge" collision are apparently more important in determining the reaction mechanism in systems with such ridges.

The motivation of this work is then to develop a dynamical picture of the cyclopropyl ring-opening reaction in light of our previous model studies. Following Mann et al.,[27,28] we use direct dynamics calculations. We treat the molecule as a classical dynamical system rather than attempting to connect our simulations to experimental or ideal T = 0 K conditions.[5,6,43] The long-standing question of zero-point energy (ZPE) and quantum mechanical effects are not considered in any detail. (A discussion of the enhancement of regular dynamics that might result from omission of ZPE is given in ref 44.) Additionally, we consider the manifestations of dynamical effects on product selectivity and in the presence of dissipative surroundings. We analyze the cyclopropyl radical ring-opening, often using the concepts and intuition developed in our 2d model study. We consider which elements of the dynamics and reaction mechanism in the 2d model are preserved in the higher dimensional ring-opening reaction and, more generally, evaluate the use of simple low-dimensional models as tools to understand and predict nonstatistical phenomena in chemical reactions.

SIMULATION METHODOLOGY

***Ab Initio* Methods.** The multiconfigurational character of both the allyl radical and the ring-opening transition state is well-documented.[10,45,46] Therefore, all[47] *ab initio* calculations reported here, save for the conical intersections, were performed with CASSCF(3,3) and the 6-31+G(d,p) basis set using the GAMESS quantum chemistry package.[48,49] The energy barrier heights for the cyclopropyl ring-opening and a single CH_2 rotation in the allyl radical product, 20.67 and 12.60 kcal mol^{-1}, respectively, calculated with CASSCF(3,3)/6-31+G(d,p) give qualitative agreement with experimental values, 23[5−7] and 15.7 kcal mol^{-1},[50] respectively. The exothermicity of 36.76 kcal mol^{-1} is somewhat larger than results computed with more sophisticated *ab initio* methods,[9,12,13,51] and the discrepancy is likely due to the neglect of dynamical electron correlation in the CASSCF(3,3) method. However, the CASSCF(3,3)/6-31+G(d,p) potential energy surface seems to capture essential features of the ring-opening process and is used in this work.

Reduced Dimensional PES and Important Coordinates. The cyclopropyl radical system contains 24 (18 internal) degrees of freedom, and the direct dynamics trajectories have full dimensionality. However, only a subset of the molecular motions are important in the ring-opening process. These "active" degrees of freedom notably include the two dihedral angles formed between the two CH_2 planes and the 3C plane and the bond angle describing the breaking of the C−C bond between the two CH_2 groups. Many of the results in this work will be presented in terms of three coordinates α, $\phi_\perp$, and $\phi_\backslash$ that represent these active degrees of freedom and have been used in theoretical studies of cyclopropane[52−54] and cyclopropylidene.[55] The bond angle between the three carbons, with the methine carbon as the vertex, is denoted α. The dihedral angles $\phi_\perp$ and $\phi_\backslash$ are those made between the *perp*-CH_2 and *tilt*-CH_2 planes, respectively, and the 3C plane. These dihedrals are not defined in the usual way in terms of the positions of four atoms[56] but are computed as the dihedral angle between the normal to the CH_2 plane and the normal to the 3C plane. The coordinates are shown in Figure 1 in a schematic of the ring-opening TS. The conrotatory mechanism occurs when $\phi_\perp$ and $\phi_\backslash$ both increase or both decrease, whereas the disrotatory mechanism occurs when $\phi_\perp$ decreases and $\phi_\backslash$ increases, or vice versa.

To visualize the PES landscape of the ring-opening, a 3d reduced dimensional PES (rd-PES) was constructed in terms of the coordinates (α, $\phi_\perp$, $\phi_\backslash$) . The energies used to fit the rd-PES were obtained on a 3d grid of (α, $\phi_\perp$, $\phi_\backslash$), the rd-PES coordinates, where constrained optimizations were performed at each point, holding (α, $\phi_\perp$, $\phi_\backslash$) constant, at CASSCF(3,3)/6-31+G(d,p). Several additional constraints were found convenient for generating the energy grid points in our chosen coordinates: (i) the methine hydrogen was restricted to lie in the 3C plane and (ii) the perpendicular distance between the 3C plane and a CH_2 hydrogen was the same for both hydrogens on a CH_2 group although each hydrogen lies on opposite sides of the 3C plane. More details about the rd-PES are given in the Supporting Information.

It is important to note that, although the rd-PES gives insight into the PES topology relevant to the reaction dynamics, the computed dynamics still occurs in the full 48d (36d internal) phase space, and significant effects from other degrees of freedom outside our reduced dimensional space are apparent. For example, the wagging of both the CH_2 groups and the methine hydrogen is important in the dynamics (see below). Additionally, the projected dynamics in the (α, $\phi_\perp$, $\phi_\backslash$) coordinates is most easily pictured as a simple model in which the 3C plane is fixed and the CH_2 groups are two stiff "propellers" attached to the ends of the opening ring. The full dynamics in an inertial frame are much more complicated. Both CH_2 groups undergo wagging motion, and the 3C plane can change its orientation when the CH_2 groups rotate. Despite these caveats, the projection of the full dynamics into the reduced dimensional space is a powerful method to visualize both the reaction dynamics and the post-TS bifurcation in the reaction mechanism.[57,58]

Direct Dynamics. *Initial Conditions.* Trajectory initial conditions were generated under the constraint that the total angular momentum is zero, J = 0, using a variation of microcanonical normal mode sampling[59] adapted from the VENUS96 program.[60−62] Details of the sampling procedure are given in the Supporting Information.

Trajectory Propagation. The trajectories were propagated using the velocity Verlet (VV) algorithm[63] directly coded into the DRC routine[64] in the GAMESS package. The gradients needed by the VV routine were computed "on-the-fly" and a time step of 0.10 fs was found sufficient to conserve energy to approximately ±10 cm^{-1}.

Ensembles of 250 trajectories were initiated for each isotopomer of the cyclopropyl radical considered at excitation energies above the barrier of E^* = 1 and 10 kcal mol^{-1}. Trajectories were propagated both forward and backward in time, and trajectories that failed to cross from the cyclopropyl region to the allyl product region were discarded from further analysis. The E^* (1 and 10 kcal mol^{-1}) and the initial condition sampling we adopt in this study are chosen to be approximately consistent with the results on the 2d VRI model potential and to facilitate comparison between the two works. These E^* values are sufficient to address fundamental questions regarding the ring-opening mechanism such as correspondence between the dynamics and the IRC and Newtonian kinetic isotope

DOI: 10.1021/acs.jpca.5b02834
J. Phys. Chem. A 2015, 119, 6611−6630

effects. The ensemble energy values chosen are below the harmonic zero point energy (ZPE) at the ring-opening TS saddle point of ~42 kcal mol^{-1} (for the singly deuterated the harmonic ZPE is ~40 kcal mol^{-1}). Though our calculations at the chosen E^* values give a sense of the energy dependence of the ring-opening mechanism, it should also be borne in mind that the sampling scheme described in the previous section is strictly only valid in a small region about the ring-opening saddle point consistent with small E^*, and that sampling at a larger energy corresponding to the full ZPE[65,66] might wash out some of the details seen in our calculations.

Dissipation was incorporated into the equations of motion as a friction term with a dissipation coefficient γ:

$$\frac{d\mathbf{x}_i}{dt} = \frac{\mathbf{p}_i}{m_i} \tag{1a}$$

$$\frac{d\mathbf{p}_i}{dt} = -\frac{\partial}{\partial \mathbf{x}_i} V(\{\mathbf{x}_j\}) - \gamma \mathbf{p}_i \qquad i = 1, 2, ..., 8 \tag{1b}$$

The VV algorithm cannot be used to propagate a dissipative system, so we have used a second-order integration method, an analogous "dissipative"-VV algorithm,[67] to propagate the dissipative trajectories. For the dissipative trajectories propagation was terminated when the energy of the molecule fell below the CH_2 rotation barrier of the allyl radical and a definitive stereoisomer assignment could be made. An ensemble of 208 trajectories with E^* = 5 kcal mol^{-1} was used for a range of values of the dissipation parameter γ.

RESULTS AND DISCUSSION

Energetics and PES Topology. Energetics of the cyclopropyl radical ring-opening are shown in Figure 2. The ring-opening is highly exothermic and the equilibrium cyclopropyl radical geometry is 35.2 kcal mol^{-1} above that for the allyl radical. The ring-opening TS is 58.7 kcal mol^{-1} above the allyl radical and 45.2 kcal mol^{-1} above the TS saddle point for CH_2 rotation of the allyl, which lies on the ridge between possible allyl stereoisomers (the imaginary frequency at this TS is only 256i cm^{-1}), hereafter referred to as the "allyl ridge". We also show the VRI point calculated by Quapp and Bofill[15] in Figure 2 and note that its geometry is quite similar to that for the allyl CH_2-rotation TS. The values (α, $\phi_\perp$, $\phi_\backslash$) for the various important points on the PES are given in Table 1, and it

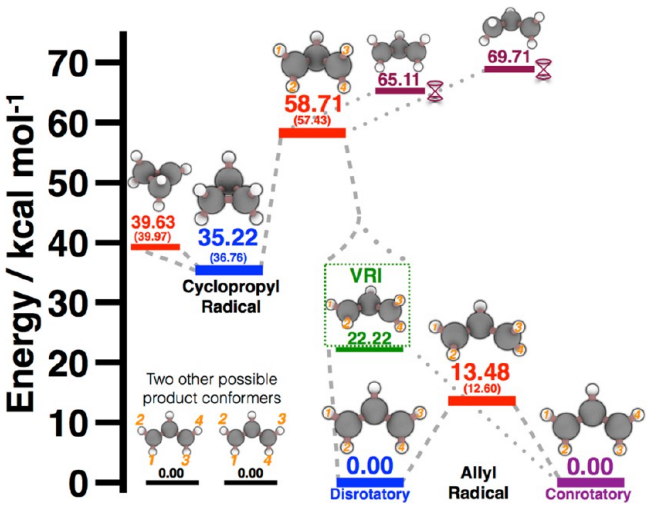

Figure 2. Stationary and other selected points, along with their corresponding energetics, on the cyclopropyl radical ring-opening reaction PES are shown. All PES values are given relative to the allyl radical and ZPE-corrected values appear in parentheses. The VRI point was taken directly from the work of Bofill and Quapp.[15]

Table 1. Coordinates of the Projections of Important Points of the Full Dimensional System Projected onto the Space of the Reduced Dimensional Potential Energy Surface[a]

	α	$\phi_\perp$	$\phi_\backslash$
cyclopropyl radical	63.6	89.5	90.5
allyl radical	124.7	0	180
ring-opening TS	90.5	84.2	116.6
CH_2-rotation TS	124.6	90.0	180.0
Q&B VRI	113.4	85.9	165.8
conical-X conrotatory	109.0	67.6	67.6
conical-X disrotatory	98.1	68.4	111.6

[a]See Figure 1 for reference. All values are given in degrees (deg).

is seen that the *tilt*-CH_2 is not completely rotated into the 3C plane at the VRI point but it is at the CH_2-rotation TS. In addition, the α coordinate is slightly smaller at the VRI point, but the *perp*-CH_2 is essentially orthogonal to the 3C plane in both structures.

Also shown in Figure 2 are the two conical intersection minimum energy crossing points (CI-MECPs) that occur between the ground and first excited electronic states, with corresponding angles of the CI-MECPs (α, $\phi_\perp$, $\phi_\backslash$) given in Table 1. As Yamaguchi[46] and Chen et al.[12] have noted, both conical intersections (CI) occur along a ring-opening coordinate with synchronous and symmetry-preserving rotations of the CH_2 groups. The conrotatory CI-MECP is higher in energy by 4.6 kcal mol^{-1} and lies above the ring-opening TS by ~11 kcal mol^{-1}. This CI-MECP resembles the allyl product more than the cyclopropyl radical and this CI has a higher-order symmetry axis, C_2, than the cyclopropyl. The disrotatory CI is of C_s symmetry and its CI-MECP resembles the cyclopropyl radical structure. The methine hydrogen remains bent out of the 3C plane in the disrotatory CI-MECP and the energy difference between this CI-MECP and the ring-opening TS is ~6.4 kcal mol^{-1}. These two PES crossings lie along the symmetry-preserving reaction paths connecting the cyclopropyl radical and the allyl radical, consistent with the predictions of the orbital correlation diagrams of Longuet-Higgins[3] which fail to connect the cyclopropyl radical and the allyl radical by a symmetry-preserving path that maintains the electronic state ordering. Even though in the present study we neglect electronically nonadiabatic effects, the presence of the CIs still has a pronounced effect on the ground state dynamics due to their influence on the topography of the ground state PES, particularly in the vicinity of the ring-opening TS.

A cut of the rd-PES with α = 93°, close to the value of the ring-opening TS, is shown in Figure 3a. The positions of the crossing seams on the rd-PES are identifiable as four sharp peaks (red color in the plot), where the high peak is the conrotatory seam and the low peak is the disrotatory seam. The ring-opening TS is situated between these two seam peaks, the three points differing primarily in their $\phi_\perp$ values (or $\phi_\backslash$ values depending on which of the four equivalent TSs one chooses). We shall consistently refer in our discussion to the ring-opening TS geometry given in Table 1. Therefore, the ring-opening reaction occurs by passing through the valley between the two

DOI: 10.1021/acs.jpca.5b02834
J. Phys. Chem. A 2015, 119, 6611−6630

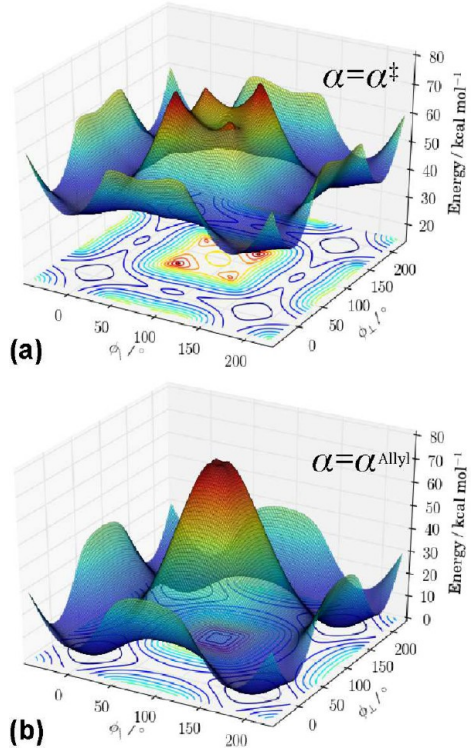

Figure 3. 3d reduced dimensional potential energy surface, rd-PES, of the ring-opening reaction defined in terms of the CH_2 dihedrals ($\phi_\perp$, $\phi_\backslash$) and the carbon backbone bond angle α. In (a) is a 2d cut of the rd-PES at the ring-opening TS value of $\alpha = 93°$, and in (b), a similar cut for the allyl product value of $\alpha = 124°$. Contour plots of the cuts are projected into the ($\phi_\perp$, $\phi_\backslash$) plane.

"mountains" of the electronic state crossings. The heights of the seam peaks, however, are different, with the disrotatory seam (that closer to the ring-opening TS) being noticeably lower in energy. The contour plot of the rd-PES with $\alpha = 93°$ is shown in Figure 4a with the regions of the four equivalent ring-opening TSs indicated by small red ovals; the proximity of the ring-opening TS to the disrotatory seam is evident. The ring-opening TS resembles the disrotatory seam structure, whereas the potential energy rises steeply between the TS and the conrotatory seam. Therefore, the local structure of the PES in the vicinity of the ring-opening TS, where the PES topography will presumably have a substantial initial influence on the dynamics, creates a slight disrotatory preference ("antidiagonal" in ($\phi_\backslash$, $\phi_\perp$) space). Trajectories passing through the TS begin closer to the disrotatory allyl radical product and have a slight tendency, particularly at lower TS excitation energy, E^*, to be "pushed" by the PES in the disrotatory direction. This disrotatory preference is accentuated in the full dimensional PES.

Figure 3b shows a 2d ($\phi_\backslash$, $\phi_\perp$) cut of the rd-PES at the allyl value of the ∠CCC, $\alpha = 124°$. The allyl radical wells occur at periodic values (in radians) of ($\pm n\pi$, $\pm n\pi$), $n = 0, \pm1, \pm2, ...$, on the 2d ϕ grid and the allyl ridge regions connect these wells via monorotations of either $\phi_\backslash$ or $\phi_\perp$. This topography is the same in both rd-PES cuts shown in Figure 3, but for $\alpha = 124°$ these wells are much lower in energy. The two rd-PES cuts shown in Figure 3 are representative of PES structures in the full-dimensional potential that play an important role in the reaction dynamics.

To help understand the electronic structure changes in the radical over the course of the reaction, and thereby some of the PES features, the three active highest energy MCSCF natural orbitals with significant population for various important points on the PES are shown in Figure 4b.

The highest doubly occupied molecular orbital (MO) in the ground electronic state (A″ symmetry) in the cyclopropyl radical is the σ bond between the two CH_2 carbons. The unpaired electron (e^-) resides in an approximately sp^3 orbital on the methine carbon with the major lobe under the methine hydrogen and 3C plane. The σ^* antibonding orbital shows small occupation from minor contributions of configuration state functions (CSFs) with a doubly occupied σ^*. The highest doubly occupied ($n = 1.83$) MO in the ring-opening TS is a "strained" σ orbital found mainly on the *tilt*-CH_2 carbon and a nascent π orbital forming between this carbon and the methine carbon. The partially formed π bond in the asymmetric structure presumably acts to stabilize the TS. Significant population is also found in the strained σ^* orbital ($n = 0.17$), where the nascent π orbital forms between the *perp*-CH_2 and methine carbons.

The multiconfigurational nature of the electronic wave function is pronounced at the ring-opening TS and several CSFs, particularly those with one electron in each active space orbital and one with a double excitation from the $\sigma \rightarrow \sigma^*$, make significant contributions.[10] This result is not unexpected given the proximity of the ring-opening TS to two CIs. The singly occupied ($n = 0.997$) orbital of the ring-opening TS shows that

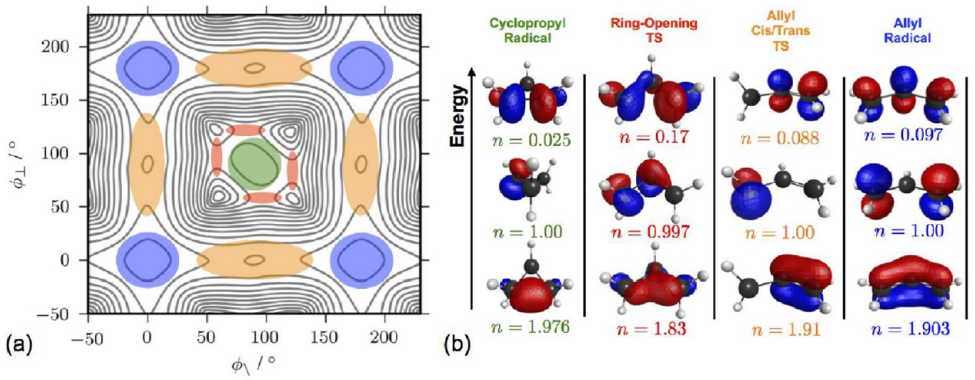

Figure 4. In (a), the different regions on the $\alpha = 93°$ cut of the rd-PES: green for cyclopropyl radical/perpendicular CH_2 groups, red for the ring-opening transition states, orange for the flat allyl ridge, and blue for the allyl radical minima. In (b), the three highest energy MCSCF natural orbitals and their occupation numbers, n, at different stationary points on the PES.

DOI: 10.1021/acs.jpca.5b02834
J. Phys. Chem. A 2015, 119, 6611−6630

the lone e^- is shifting from an sp^3 orbital on the methine carbon to an sp^3 orbital on the *perp*-CH_2. In the CH_2-rotation TS, representative of the allyl ridge, the π bond between the methine and *tilt*-CH_2 carbons is fully formed creating a stabilizing interaction. The existence of the allyl ridge is then a consequence of the stabilizing π bond formed between the methine carbon and the in-plane CH_2 carbon. The resulting allyl ridge feature is shown in orange in Figure 4a. The radical orbital in the CH_2-rotation TS is a localized sp^3 orbital on the *perp*-CH_2 carbon. The *perp*-CH_2 group in this configuration is both orthogonal to the 3C plane and significantly pyramidilized by the residing radical.

The allyl radical orbitals form the π system, with the in-phase and delocalized π orbital being doubly occupied. The radical orbital with single occupation is composed of the p orbitals of the symmetry equivalent CH_2 carbons of A_2 symmetry. A small occupation is found in the π antibonding orbital for which all the p orbitals in the π system are out of phase.

Intrinsic Reaction Coordinate. The intrinsic reaction coordinate[14,17] (IRC) of the cyclopropyl ring-opening has been considered in several other works,[9−11] and we briefly review some of the points made in those papers in the context of our study.

The IRC energetics and several projections of the IRC path into the $(\alpha, \phi_\perp, \phi_\backslash)$ coordinate space are shown in Figure 5.

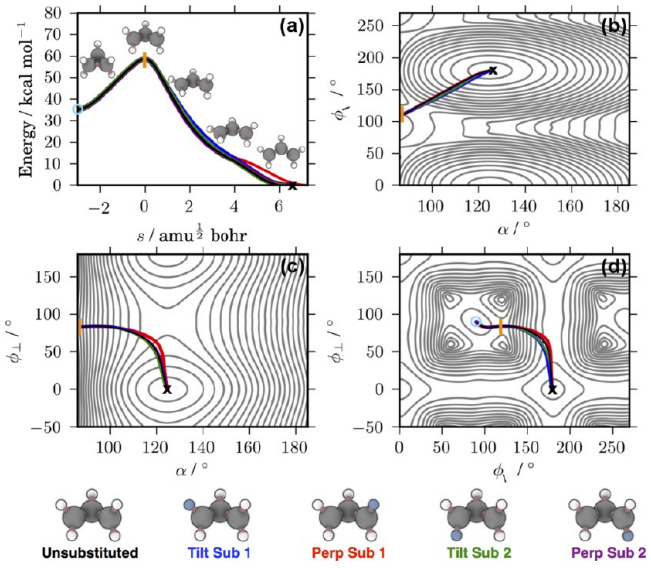

Figure 5. Intrinsic reaction coordinate (IRC), *s*, of the cyclopropyl radical ring-opening reaction is shown for various isotopomers: (a) the potential energy over the IRC, (b) the $(\alpha(s), \phi_\backslash(s))$ contour over the IRC with $\phi_\perp$ = 93° rd-PES $(\alpha, \phi_\backslash)$ contour plot background, (c) the $(\alpha(s), \phi_\perp(s))$ contour over the IRC with $\phi_\backslash$ = 180° rd-PES $(\alpha, \phi_\perp)$ contour plot background, (d) $(\phi_\backslash(s), \phi_\perp(s))$ contour over the IRC with α = 120° rd-PES $(\phi_\perp, \phi_\backslash)$ contour plot background. The positions of the cyclopropyl radical, the ring-opening TS, and the allyl product are indicated by a blue "○", an orange "|", and a black "x", respectively.

The IRC path was also calculated[68] for all singly deuterium-substituted isotopomers of the cyclopropyl radical, except for a substitution of the methine hydrogen. The large exothermicity of the ring-opening process is readily seen from the significant drop of the potential energy as the IRC proceeds from the ring-opening TS to the allyl radical product in Figure 5a. Ball-and-stick molecular models[69] are inset to indicate the configurations and participating degrees of freedom along portions of the IRC.

It is evident from Figure 5 that the IRC predicts ring-opening to occur via disrotatory rotations of the CH_2 groups. The first step of this mechanism is the simultaneous opening of the ring, as indicated by an increasing α angle, and outward rotation of the *tilt*-CH_2 group, seen clearly in Figure 5b. This simultaneous motion continues past the ring-opening TS and down onto the allyl ridge before the *perp*-CH_2 group undergoes any significant rotation. The second step of the IRC mechanism is heralded by an inflection in the energy curve in Figure 5a where the IRC path enters the allyl ridge and thus falls less steeply. Here the characteristic motion changes from the simultaneous ring-opening/*tilt*-CH_2 rotation to rotation of the *perp*-CH_2 as the *perp*-CH_2 carbon changes from sp^3 to sp^2 hybridization. In Figure 5c,d, the change in the nature of the primary IRC motion on the allyl ridge is apparent as the final approach to the allyl product is essentially the *perp*-CH_2 rotation into the 3C plane. This two-step mechanism suggests the ring-opening reaction has a great deal of asynchronous character. In a fully asynchronous ring-opening reaction, the two CH_2 groups would rotate in disjoint steps, and the IRC contour in Figure 5d would appear as a sharp right-angle turn at $\phi_\backslash$ = 180° toward the allyl product. However, some synchrony is apparent, as the turn toward the allyl product is more gradual than a perpendicular change in direction.

The effect of single deuterium substitution on the IRC depends upon the substitution location. If the substitution occurs on the *tilt*-CH_2 group, the blue and green curves in Figure 5, the inflection of the energy on the allyl ridge of the IRC is less pronounced, and the IRC avoids a portion of the allyl ridge traversed in the unsubstituted case. The deuterium substitution on the *tilt*-CH_2 group causes the IRC to correspond to more synchronous motion. This effect is seen in Figure 5d where the blue and green curves have a gentler curvature than the black curve. In contrast, substitution of the "top" hydrogen, that on the same side of the 3C plane as the methine hydrogen, on the *perp*-CH_2 group shifts the IRC to a more asynchronous path. This substitution takes the IRC farther into the allyl ridge than the other substitutions. Substitution of the "bottom" hydrogen of the *perp*-CH_2 has very little effect on the IRC path relative to the unsubstituted isotopomer, and in most of the panels of Figure 5, the purple curve corresponding this isotopomer lies under the black curve of the unsubstituted radical. None of the substitutions studied in this work change the IRC to a conrotatory path. Nevertheless, the qualitative changes in character of the IRCs depending on the location of the d-substitution are reflective of a significant classical mechanical isotope effect in the dynamics.[58]

Ring-Opening Dynamics. *Preliminary Discussion.* If the hydrogens on the CH_2 groups are treated as distinguishable, then there are four isoenergetic C_1 ring-opening TSs (Figure 6). If the hydrogens are treated as indistinguishable, then there are only two distinct chiral ring-opening TSs. We will study the dynamics of trajectories initiated from one of the ring-opening TSs, given in Table 1, and consider all the hydrogens to be distinguishable. Though we will refer to stereoisomers, as shown on the bottom of Figure 2, such products are not experimentally distinguishable when the CH_2 groups can undergo facile internal rotation.

With the single CH_2-group deuterium substitutions, there are two experimentally distinguishable allyl radical products, *cis* and

DOI: 10.1021/acs.jpca.5b02834
J. Phys. Chem. A 2015, 119, 6611−6630

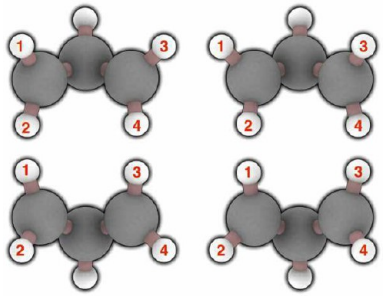

Figure 6. Four equivalent transition states of the cyclopropyl radical ring-opening related by feasible permutations of the CH_2 hydrogens. The ring-opening transition states are chiral.

trans. We shall nevertheless treat as distinguishable the four possible singly deuterated allyl products, two *cis* and two *trans*.

Determining when a trajectory has passed through the ring-opening TS dividing surface to its associated allyl radical stereoisomer product is essential in deciding whether the trajectory corresponds to a con- or disrotatory mechanism. However, any practical definition of the allyl product region is subject to some ambiguity. Figure 7 shows our chosen allyl

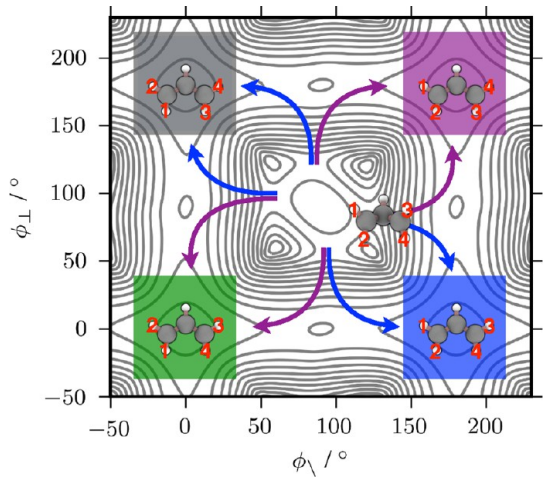

Figure 7. Configuration space divisions used to assign the product allyl radical stereoisomers are shown inset on the contours of the rd-PES with $\alpha = 93°$ projected into the $(\phi_\backslash, \phi_\perp)$ plane. The location of the ring-opening TS where the trajectories are initialized is also indicated.

product definition, where product assignment is made when a trajectory is in a region of $(\alpha, \phi_\perp, \phi_\backslash)$ configuration space where $\alpha > 95°$ and both $\phi_\backslash$ and $\phi_\perp$ are within $\pm\phi_{cutoff}$ of an allyl stereoisomer for which both ϕ angles must be an integer multiple of π; i.e., the allyl stereoisomer product configuration space region is a square in the ϕ angles space with sides of length $2\phi_{cutoff}$. We chose ϕ_{cutoff} so that (i) the first allyl stereoisomer formed must be one of the two connected by the allyl ridge immediately entered after passing the ring-opening TS dividing surface surface and (ii) trajectories must traverse at least some portion of the allyl ridge prior to product assignment. Several values of ϕ_{cutoff} were tested, but we shall only discuss values 30° and 45°, primarily the former, which we have found to give meaningful results and product assignments approximately independent of ϕ_{cutoff} for the chosen E^* ensembles of this study.

A trajectory is classified as con- or disrotatory on the basis of the first allyl stereoisomer region it enters. Below, we shall note cases when our chosen method of product assignment becomes poorly defined; such a breakdown signals interesting mechanistic information as well as the inherent limitations of the assignment criteria.

When deuterium substitutions are made and the isoenergetic ring-opening TSs become unique, the free energy differences between these TSs are quite small, $<k_BT$ for ambient temperatures, e.g., ∼50 cm^{-1} at T = 298 K for single substitutions on the CH_2's. Any observable nonstatistical effects require that the reaction dynamics is highly specific to an individual TS. Complications related to symmetry and TS near-degeneracy can be removed by a halogen substitution on the CH_2's that will separate the possible TSs in energy, and such a system may be more suited for experimental study.

Unsubstituted Isotopomer. Both con- and disrotatory trajectories are observed in simulations of the ring-opening of the cyclopropyl radical for both the E^* = 1 and 10 kcal mol^{-1} ensembles. The ensemble fraction of con- and disrotatory events are given in Table 2 where it is seen that the disrotatory mechanism is dominant in both ensembles. The 2d projections of the trajectory paths are shown in Figure 8 for (a) E^* = 1 kcal mol^{-1} and (b) E^* = 10 kcal mol^{-1}, over the first 100 fs after the trajectories cross the ring-opening TS. In the $(\alpha, \phi_\backslash)$ plane, the trajectories closely follow the IRC projection to their approximate values at the allyl product. During the initial phase of the ring-opening dynamics, the trajectories in both ensembles follow very similar paths because the large force acting during the fall from the ring-opening TS to the allyl ridge, Figure 5, overwhelms motion transverse to the IRC.[70] In *all* the trajectories, the *tilt*-CH_2 group initially rotates by increasing $\phi_\backslash$ until the CH_2 group lies in the 3C plane, consistent with the IRC and the previous observations of Mann and Hase.[27] The rotation of the *tilt*-CH_2 group occurs simultaneously with the opening of the carbon backbone and the rotation of the methine hydrogen into the 3C plane. Therefore, the reaction path bifurcation of the cyclopropyl radical ring-opening is associated with neither the opening of the carbon backbone nor the rotation of the *tilt*-CH_2.

Table 2. Fraction of Disrotatory and Conrotatory (Given as "dis:con") in Each Ensemble[a]

	E^* = 1 kcal mol^{-1}		E^* = 10 kcal mol^{-1}	
ensemble	ϕ_{cutoff} = 30°	ϕ_{cutoff} = 45°	ϕ_{cutoff} = 30°	ϕ_{cutoff} = 45°
H (250/255:213/250)	0.676:0.324	0.68:0.32	0.67:0.33	0.67:0.33
*d*1 (237/250:227/250)	1.0:0.0	1.0:0.0	0.80:0.20	0.80:20
*d*2 (240/250:210/250)	0.15:0.85	0.15:0.85	0.38:0.62	0.40:0.60
*d*3 (240/250:229/250)	1.0:0.0	1.0:0.0	0.78:0.22	0.80:0.20
*d*4 (243/250:214/250)	0.74:0.26	0.93:0.07	0.64:0.36	0.72:0.28

[a]The number of reactive/total trajectories in each ensemble is also given (E^* = 1 and 10 kcal mol^{-1}).

DOI: 10.1021/acs.jpca.5b02834
J. Phys. Chem. A 2015, 119, 6611−6630

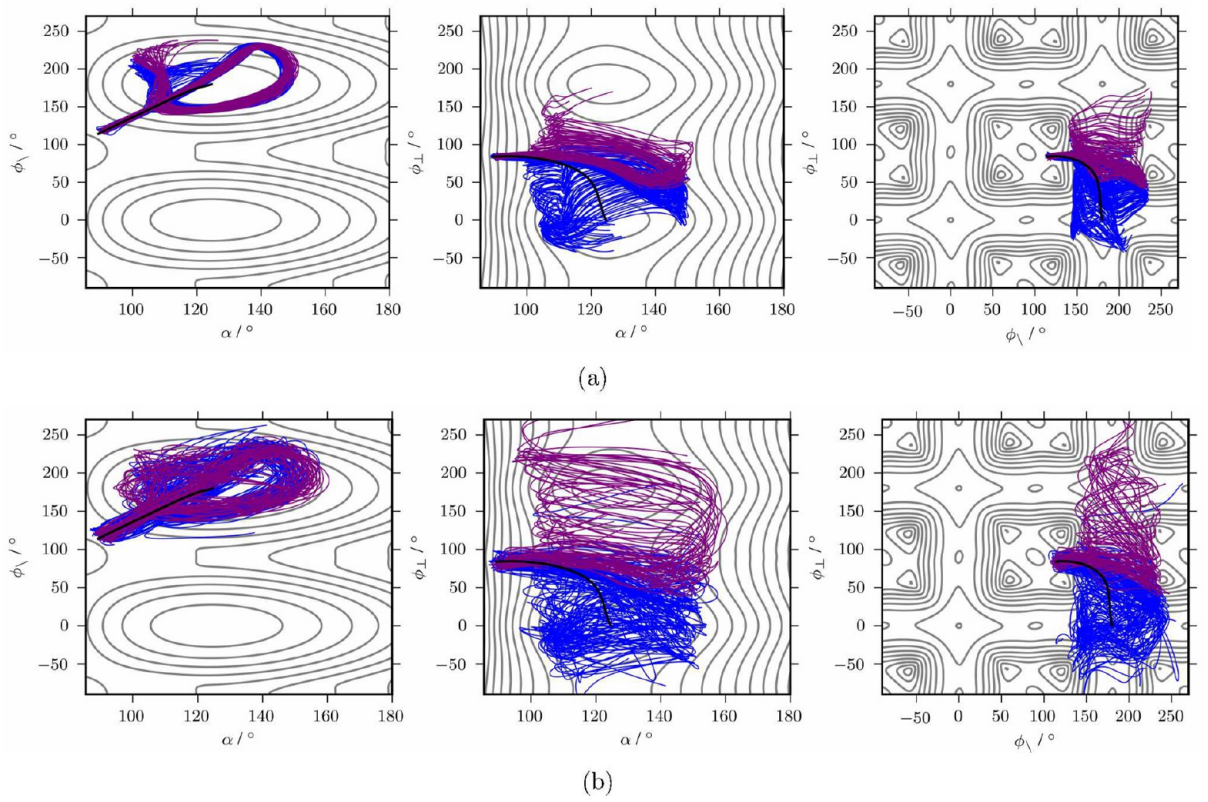

Figure 8. Full dimensional trajectories projected into the (α, $\phi_\backslash$), (α, $\phi_\perp$), and ($\phi_\backslash$, $\phi_\perp$) spaces (left, middle, and right panels, respectively) for propagation times between 0 (the ring-opening TS crossing time) and 100 fs from the initial sampled barrier crossing. Disrotatory trajectories are shown in blue and conrotatory trajectories are shown in purple. In (a), the E^* = 1 kcal mol^{-1} ensemble is shown and in (b) E^* = 10 kcal mol^{-1} ensemble is shown. The IRC projected into the various coordinate spaces is shown in black.

Rotation of the *perp*-CH_2 group occurs primarily when trajectories reach the allyl ridge region of the PES and determines whether a given trajectory is classified as either con- or disrotatory. In the center and rightmost columns of Figure 8, the initial deviation of the dynamics from the IRC is evident. Large momenta associated with initially excited large amplitude coordinates cause trajectories to bypass this synchronous portion of the path, often without the mechanism-determining motion in $\phi_\perp$ occurring. As the trajectories pass over the allyl ridge region and subsequently collide with the potential wall, the $\phi_\perp$ degree of freedom is activated. The *tilt*-CH_2 and methine hydrogen rotations/bends play a prominent role in the subsequent dynamics. These degrees of freedom and α tend to oscillate with relatively large amplitude about their allylic equilibrium values as the *perp*-CH_2 undergoes its mechanism-determining motion into the 3C plane.

In our work[25] on the model 2d PES with a bifurcating reaction path, it was seen that the initial product was strongly influenced by where the trajectories collided with the potential wall after passing over the ridge. It was found that the shape of the potential at this collision point directed the trajectories toward a particular product (or back over the initial TS, though we observed no trajectories that reentered the cyclopropyl reactant region after reaching the allyl ridge). "Over-the-ridge" collisions play an evident role in the cyclopropyl ring-opening as well. In the last column of Figure 8, the turning point in the $\phi_\backslash$ motion is clearly discernible, whereas from the first column of Figure 8 it is evident that $\phi_\backslash$ reaches its turning point before α. Conrotatory trajectories tend to undergo this collision at higher values of $\phi_\perp$, which subsequently causes them to move toward the conrotatory product. The fastest reacting disrotatory trajectories proceed from this "over-the-ridge" collision into the disrotatory allyl well.

In the 2d VRI model, the trajectories passed over the ridge region in essentially straight-line motion and the directionality following the initial collision was apparent. The cyclopropyl ring-opening trajectory paths, as projected onto the 2d contour plots of the rd-PES, are more complicated and other degrees of freedom besides α, $\phi_\backslash$, and $\phi_\perp$ contribute to the dynamics. The concept of an "over-the-ridge" collision in the higher dimensional dynamics is therefore somewhat ambiguous, but we shall take it to mean the interval in the dynamics where $\phi_\backslash$ and α (and the *perp*-CH_2 wag) reverse their initial direction. In the center and right panels of Figure 8, most apparent for the E^* = 1 kcal mol^{-1} ensemble, trajectories initially passing over the allyl ridge appear to "bend" anomalously to lower values of $\phi_\perp$ prior to the over-the-ridge collision. This bend occurs after the trajectories pass through the vicinity of the VRI point, but farther along in the motion and much more weakly than the corresponding bend on the IRC. Animations of trajectories (Figure 9) suggest that this "disrotatory bend" begins before the *tilt*-CH_2 and the methine hydrogen fall into the 3C plane to form a C−C π bond. The origin of the disrotatory bend is that, in the lab frame, as the *tilt*-CH_2 and methine hydrogen rotate into and below the 3C plane, the 3C plane rotates upward in the lab frame to conserve angular momentum while the *perp*-CH_2 remains approximately orthogonal to the initial orientation of the 3C plane.

The wagging of the *perp*-CH_2 group, i.e., the motion of both hydrogens in the same direction orthogonal to the CH_2 plane

DOI: 10.1021/acs.jpca.5b02834
J. Phys. Chem. A 2015, 119, 6611−6630

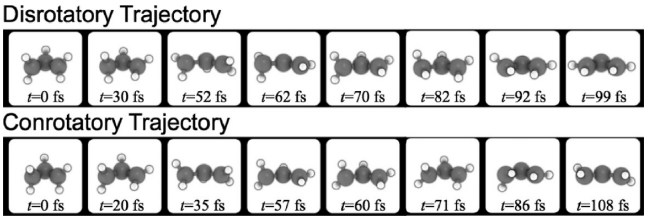

Figure 9. Example dis- and conrotatory trajectories in the E^* = 10 kcal mol^{-1} ensemble are shown as snapshots at various propagation times. The molecules have been oriented for better visualization.

and the movement of the CH_2 carbon in the opposite direction, plays an important role in the initial dynamics. This large amplitude motion gains significant excitation on the initial descent from the ring-opening TS barrier. The *perp*-CH_2 wag is one of the highly coupled degrees of freedom involved in both the "over-the-ridge" collision and the disrotatory bending described in the previous paragraph. It also is not accurately accounted for in the rd-PES model. Parts a and b of Figure 10 show average wag angles θ, defined to be the angle between the CH_2-group plane and its connecting C−C bond, for both E^* ensembles. The wag of the *tilt*-CH_2 group, $\theta_\backslash$, remains relatively unexcited during the first ∼100−150 fs. The reason for the excitation of the *perp*-CH_2 wag is clear if one animates a trajectory, Figure 9. The *perp*-CH_2 carbon atom participates in the initial ring-opening by moving outward toward a larger α bond angle. The *perp*-CH_2 hydrogens do not respond immediately to the movement of their carbon atom anchor, which can be seen in Figure 10a,b. When the *perp*-CH_2 carbon atom has moved sufficiently far from its attached hydrogens, it abruptly "pulls" the hydrogens along with it. As the *perp*-CH_2 carbon reaches the apex in α the *perp*-CH_2-wagging motion has a large amount of momentum due to the prior pull from the carbon. The *perp*-CH_2 hydrogens, therefore, continue their outward motion toward increasing $\theta_\perp$ until they reach a turning point at a highly distorted geometry (see the first sharp increase in $\theta_\perp$ in Figure 10). Parts c and d of Figure 10 show the wag angles of *perp*-CH_2 for each ensemble resolved into the dis- and conrotatory trajectories. The excitation of the *perp*-CH_2 wag is common to both the dis- and conrotatory mechanisms.

In Figure 10a,b, the CH_2-wag motions are seen to be highly coherent over a ∼150 fs time scale during which the ring-opening reaction takes place. Excitation in the *perp*-CH_2 wag persists despite the fact that many of the trajectories have formed, at least transiently, one of the allyl stereoisomers by this time. The excitation of the *perp*-CH_2 wag is greater at higher E^*, and the energy transfer to the *perp*-CH_2 wag may be more efficient when the internal motions of the system begin "colder".

To summarize, the effects from the degrees of freedom not contained in the set of key coordinates (α, $\phi_\backslash$, $\phi_\perp$) are seen to have a significant contribution to the dynamics, particularly at times near and during the over-the-ridge collision event. At this point in the dynamics the momenta in the degrees of freedom excited during the descent from the ring-opening TS barrier have carried the trajectories into regions of configuration space corresponding to highly distorted geometries on the allyl ridge far from the IRC. In these regions, the large amplitude motions are highly coupled and the 3d model picture in the key coordinates is of limited use. The omission of important large amplitude motions from the 3d reduced dimensional (α, $\phi_\backslash$, $\phi_\perp$) model of the cyclopropyl radical ring-opening reaction raises the question of which essential dynamical features are contained or are missing from such a simplified model[25,52−54] and, indeed, from a traditional and intuitive picture of ring-opening reactions.

The evolution of the $\phi_\backslash$ and $\phi_\perp$ angles for a few sample trajectories in the E^* = 1 kcal mol^{-1} ensemble is shown in

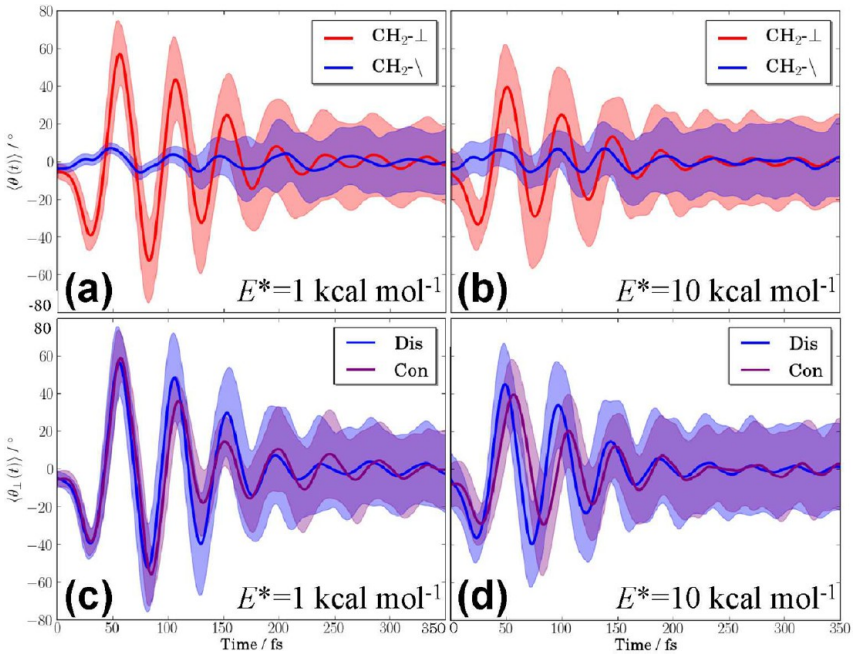

Figure 10. Average carbon pyramidalization angle, θ, versus time for the (a) E^* = 1 kcal mol^{-1} and (b) E^* = 10 kcal mol^{-1} ensembles (red for *perp*-CH_2, blue for *tilt*-CH_2). *perp*-CH_2-pyramidilization angle time series averaged over the disrotatory (blue) and conrotatory (purple) trajectories for the (c) E^* = 1 kcal mol^{-1} and (d) E^* = 10 kcal mol^{-1} ensembles. Error bars about $\langle\theta(t)\rangle$ angles are given in each plot as $\pm\sigma(t)$, where $\sigma(t)$ is the ensemble standard deviation.

DOI: 10.1021/acs.jpca.5b02834
J. Phys. Chem. A 2015, 119, 6611−6630

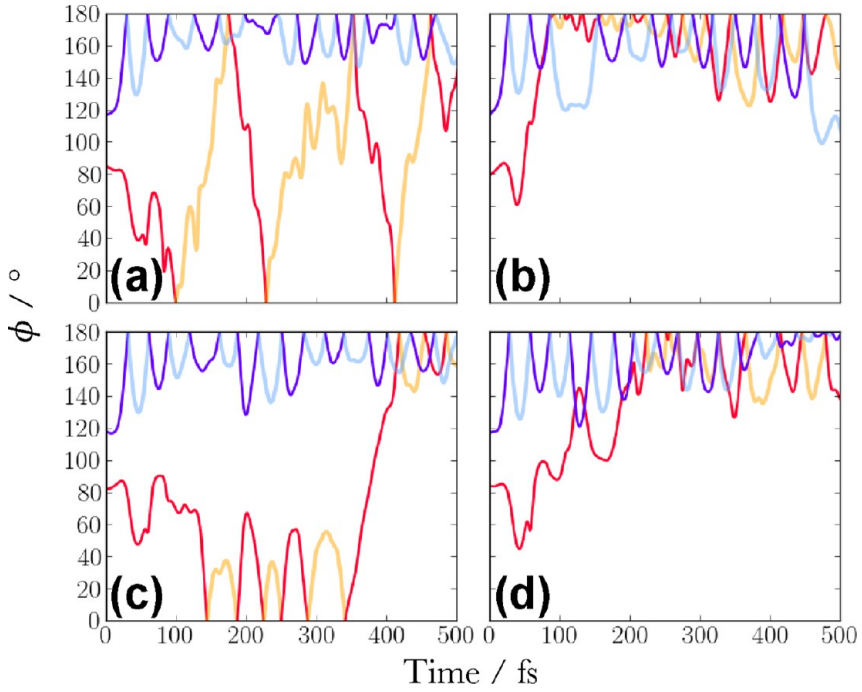

Figure 11. $\phi_\perp$ (red) and $\phi_\backslash$ (blue) coordinates for example trajectories (a)−(d) in the E^* = 1 kcal mol^{-1} ensemble versus propagation time. The faded colors indicate when the ϕ coordinates are larger than 180° or less than 0°, and the coordinates are defined as in Figure 1.

Figure 11. The initial decrease in $\phi_\perp$ is seen in all the trajectories and the first minimum of $\phi_\perp$ occurs during the over-the-ridge collision event. In all the trajectories shown, $\phi_\perp$ then rotates back into the allyl ridge direction with different outcomes for each of the trajectories. In Figure 11a, the more typical, disrotatory trajectory undergoes the over-the-ridge collision at small $\phi_\perp$, and the *perp*-CH_2 rotates into the disrotatory allyl product. In Figure 11c, the back rotation of $\phi_\perp$ is sufficient for the trajectory to reenter the allyl ridge. This trajectory becomes trapped in the allyl ridge region while the $\phi_\backslash$ coordinate undergoes ∼1 oscillation before falling into the disrotatory product region. In the short conrotatory trajectory in Figure 11b, the initial over-the-ridge collision occurs at a higher value of $\phi_\perp$ and back-rotation after the initial drop in $\phi_\perp$ causes the trajectory to head directly to the conrotatory product. The conrotatory trajectory in Figure 11d undergoes complicated motion in $\phi_\perp$ after the back-rotation and undergoes oscillations in the region between 90° and 180° before finally passing definitively into the conrotatory allyl product region. Although subsequent *tilt*-CH_2 rotation does not occur in these example trajectories, such events did occur in the ensembles.

The ring-opening process in both E^* ensembles is essentially complete ∼200 fs after crossing the ring-opening TS. In Figure 12, the cumulative reaction event probability, defined by[71]

$$P(t) = \frac{1}{N_{\text{Traj}}} \sum_{i=1}^{N_{\text{Traj}}} \Theta(t - t_i^{\text{rxn}}) \tag{2}$$

is shown, where N_{Traj} is the number of reactive trajectories in the ensemble, t_i^{rxn} is the reaction time of trajectory i, and Θ is the Heaviside function. The reaction time is defined by the time at which both $\phi_\backslash$ and $\phi_\perp$ are first within $\pm\phi_{\text{cutoff}}$ of an allyl product stereoisomer configuration. Although the shapes of the distributions in Figure 12 are sensitive to the chosen value of ϕ_{cutoff} in the range 30−45° (the 30° distribution rises more

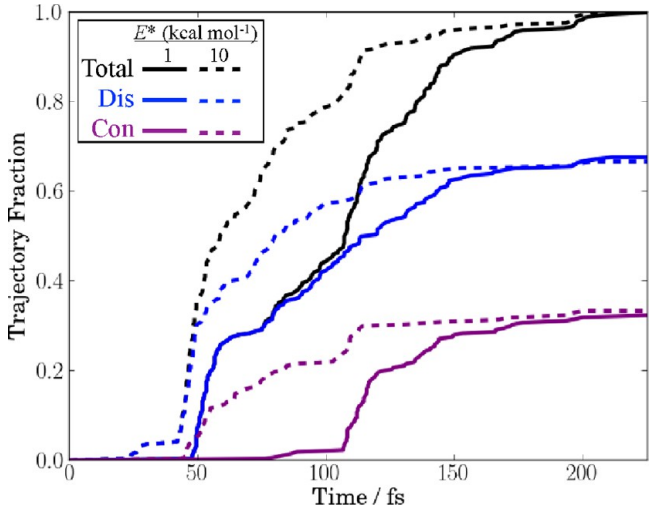

Figure 12. Cumulative probability distribution of allyl radical product formation, defined to be the first time at which both CH_2 groups make a dihedral angle with the 3C plane less than 30°. Product distributions for the disrotatory (conrotatory) events are shown in blue (purple). The E^* = 1 kcal mol^{-1} ensemble is shown with solid lines and E^* = 10 kcal mol^{-1} ensemble is shown with dashed lines.

gradually), the dis- to conrotatory ratio is approximately constant; see fractions Table 2.

Several mechanistic conclusions are apparent. First, the disrotatory mechanism is associated with a shorter time scale primarily due to the trajectories being directed toward the disrotatory product by the shape of the PES at the ring-opening TS and subsequently by forces on the allyl ridge. Conrotatory trajectories start out heading toward the disrotatory product but then must reverse their motion in $\phi_\perp$ and traverse the allyl ridge.

For E^* = 1 kcal mol^{-1} the conrotatory reaction occurs on a time scale of ∼125 fs, approximately 75 fs longer than the first

DOI: 10.1021/acs.jpca.5b02834
J. Phys. Chem. A 2015, 119, 6611−6630

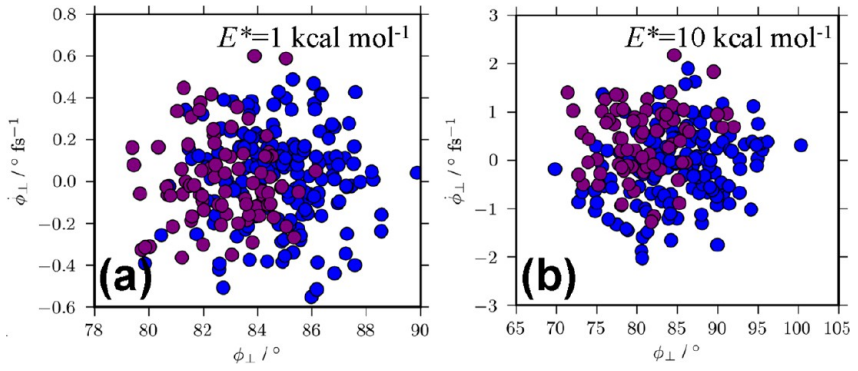

Figure 13. Initial conditions of $\phi_\perp$ and its velocity, t = 0 fs, in the sampled ensemble for (a) E^* = 1 kcal mol^{-1} and (b) E^* = 10 kcal mol^{-1}. Disrotatory (conrotatory) trajectories are shown in blue (purple).

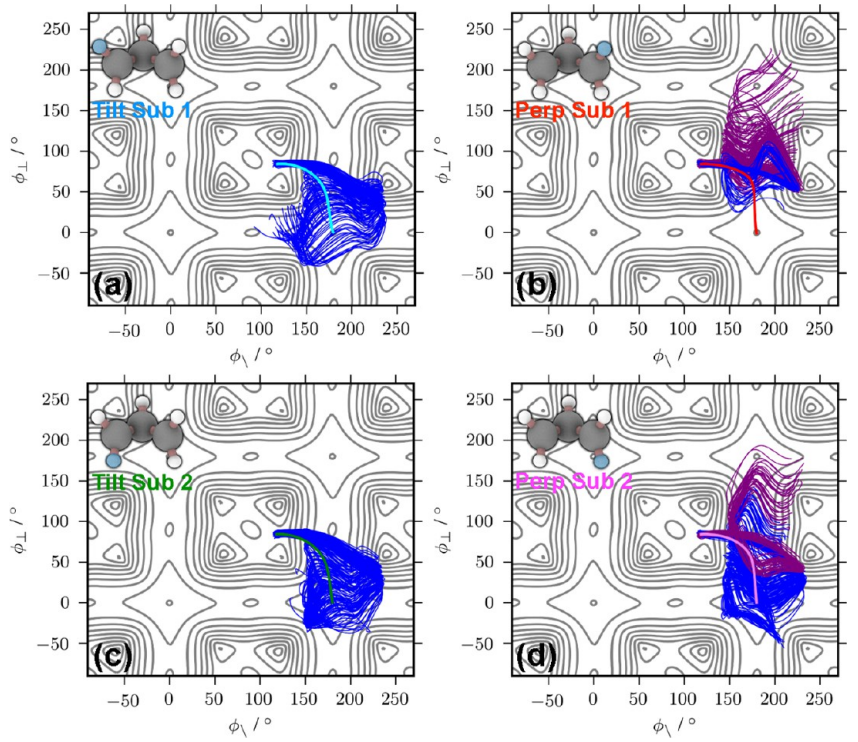

Figure 14. Full dimensional trajectories projected into the ($\phi_\backslash$, $\phi_\perp$) space for propagation times between 0 (the ring-opening TS crossing time) and 100 fs for the E^* = 1 kcal mol^{-1} ensemble for each of the four (a–d) CH_2 singly deuterated isotopomers of the cyclopropyl ring-opening TS. The top (bottom) row plots correspond to d-substitutions on the "top" ("bottom") hydrogens. The left (right) column plots correspond to d-substitutions on the *tilt*-CH_2 (*perp*-CH_2).

pulse of disrotatory trajectories. For E^* = 10 kcal mol^{-1}, not only do the con- and disrotatory distributions occur on shorter time scales but also the time scale disparity between the two mechanisms is significantly reduced. These differences in reaction time scales are of dynamical origin. At higher E^*, trajectory ensembles have a larger accessible phase space for crossing the ring-opening TS dividing surface so that trajectories are not necessarily initiated close to the IRC at the barrier. The greater dynamical diversity at the ring-opening TS crossing and the ability of trajectories to resist deflections on the PES at higher E^* allows entrance into the allyl ridge in a region further displaced from the disrotatory product than at lower ensemble energy. This results in the faster conrotatory time scale and higher fraction of conrotatory trajectories in the E^* = 10 kcal mol^{-1} ensemble relative to the E^* = 1 kcal mol^{-1} ensemble. In contrast, at higher E^* a greater number of trajectories enter the allyl ridge region closer to the disrotatory product and the number of direct disrotatory trajectories increases. Such direct trajectories shorten the characteristic disrotatory time scale at higher E^*, as seen in Figure 12. The dis- to conrotatory ratio of ∼2:1 is the same for both E^* = 1 and 10 kcal mol^{-1}, but this is within the error bars associated with the small ensemble sizes and the quality of the ring-opening TS dividing surface providing the initial conditions. The disrotatory mechanism, however, is clearly preferred at both energies.

The reaction time cumulative distributions in Figure 12 reveal that reaction events essentially occur in two pulses. The first pulse is primarily composed of disrotatory trajectories and results from "direct" reactions where energy transfer into the $\phi_\perp$ coordinate is more efficient. These trajectories undergo no, or very few (∼1), oscillations within the allyl ridge region

DOI: 10.1021/acs.jpca.5b02834
J. Phys. Chem. A 2015, 119, 6611−6630

before being classified as reactive. The second pulse is due to "indirect" trajectories that spend some time undergoing reflections in the allyl ridge region before crossing a ϕ_{cutoff} boundary to a product region with a characteristic reaction time of >75 fs (Figure 12). Both the con- and disrotatory mechanisms have direct and indirect contributions. However, the direct component is strongly favored for higher E^* and for the disrotatory mechanism.

To investigate the differences between the dis- and conrotatory trajectories at the crossing of the ring-opening TS, we looked at the α, $\phi_\backslash$, and $\phi_\perp$ initial ($t = 0$) coordinates and velocities on the sampled nominal ring-opening TS dividing surface. Only the $\phi_\perp$ initial conditions showed a discernible pattern and we plot the initial condition points on the $(\phi_\perp, (d/dt)\phi_\perp)$ plane for both the $E^* = 1$ and 10 kcal mol^{-1} ensembles in Figure 13a,b, respectively. Though little can be concluded about the distribution of disrotatory trajectories, the conrotatory trajectories favor smaller $\phi_\perp$ values on the ring-opening TS crossing. Whether this simple correlation between the ring-opening TS dividing surface $\phi_\perp$ distribution and mechanism classification is maintained at higher E^* is unknown, but exploratory calculations on an ensemble at $T = 447$ K (Supporting Information) seem to show an analogous effect.

In their study,[27] Mann and Hase observed some correspondence between the energy in the reaction coordinate on the ring-opening TS crossing and the con- or disrotatory mechanism.[27] They noted that disrotatory trajectories tended to have greater energy in the reaction coordinate on the crossing of the ring-opening TS whereas conrotatory trajectories tended to have less. We did not observe such a correlation between the dis- or conrotatory classification and the initial reaction coordinate energy, and moreover, we observed no clear relation between the observed mechanism ratio and the distribution of energy in any of the other barrier normal modes composing the sampled dividing surface. We note that we have used far smaller excitation (E^*) energies than Mann and Hase, though our preliminary work on the $T = 447$ K ensemble does not seem to show any dependence on the initial reaction coordinate crossing energy. From the ensembles presented here, it appears that the initial position and velocity of $\phi_\perp$ is more indicative, though not determining, of the dis- to conrotatory mechanism division than the energy in the ring-opening-reaction motion at the ring-opening TS.

Singly d-Substituted Isotopomers. Kinetic isotope effects (KIEs) are usually considered to have a quantum mechanical origin: either (i) isotopic substitution changes the relative zero point energy difference of the TS and the reactants or (ii) tunneling is more significant for the lighter isotope. However, the work of Singleton and co-workers[58,72,73] has shown the existence of a classical, or "Newtonian", KIE in several example organic reactions exhibiting reaction path bifurcations where the KIE influences product selectivity.

The cyclopropyl ring-opening TS is of C_1 symmetry and the IRC is disrotatory under all single d-substitutions of the CH_2 groups, so this reaction lacks the symmetry of the systems studied by Singleton. Nevertheless, a Newtonian isotope effect is evident in the initial dynamics of the cyclopropyl ring-opening process. In Figure 14a–d, the $E^* = 1$ kcal mol^{-1} trajectories are shown in the $(\phi_\backslash, \phi_\perp)$ plane over the first 0–100 fs for each possible single D-substitution of the CH_2 groups. The dis- to conrotatory trajectory fraction in the ensembles is given in Table 2, where it can be seen that the d-substitution of the top hydrogen on the *tilt*-CH_2 group results in the complete elimination of the conrotatory mechanism in the $E^* = 1$ kcal mol^{-1} ensemble within the uncertainty of the given sampling scheme. Trajectories, however, do not track along the IRC as they enter the allyl ridge region and so undergo over-the-ridge collisions just as in the unsubstituted ensemble. The bending toward smaller values of $\phi_\perp$ is more pronounced for the top *tilt*-CH_2 substitution than for the unsubstituted radical, with many of the trajectories bent either into or in close proximity to the disrotatory allyl product region on the initial opening, Figure 14a. The deuterium substitution on the *tilt*-CH_2 slows the initial dynamics and increases the magnitude of the 3C plane disrotatory bend effect. The d-substitution on the *tilt*-CH_2 increases this group's inertia and hence the time required for the ring-opening and the *tilt*-CH_2 initial rotation. This not only accentuates the disrotatory bend but also slows the initial ring-opening, prolonging disrotatory forces acting on the *perp*-CH_2. The favored mechanism is then the disrotatory rotation similar to the IRC. From Figure 14c, it can be seen that d-substitution of the bottom hydrogen of the *tilt*-CH_2 group has a very similar result to the top d-substitution, for analogous reasons.

The d-substitution of the top hydrogen of the *perp*-CH_2 (*perp*-DCH) causes a drastic change in the ring-opening mechanism where, in the $E^* = 1$ kcal mol^{-1} ensemble, the conrotatory opening is now favored by a factor greater than ~5. In Figure 14b, the disrotatory bend is less prominent in *perp*-DCH than in either d-substitution of the *tilt*-CH_2. As the ∠CCC increases and the *perp*-CH_2-wag motion is induced, the inertia of the top deuterium results in a smaller acceleration of that atom and a decrease in the amount of excitation in the *perp*-DCH wag relative to the unsubstituted ring-opening. In contrast, the lighter bottom *perp*-DCH hydrogen has a greater response to the ring-opening and, while remaining under the 3C plane, accelerates more quickly when "tugged" by its attached carbon during the initial ring-opening. The effect is that the top deuterium comes closer to the inside of the opened ring while the bottom hydrogen becomes closer to the outside of the opened ring, i.e., closer to the conrotatory configuration. The result is a strong conrotatory bias in the initial dynamics.

In the simplest and fastest conrotatory trajectories, the initial conrotatory bias is sufficient to direct trajectories into the conrotatory (*cis*) allyl product region. For most of the trajectories, however, this is followed by the onset of complicated motion in the allyl ridge region, with several bends in the trajectories occurring on the ridge, as seen in Figure 14b. A majority of these trajectories eventually enter the conrotatory *cis* product region after ~3 turning points in $\phi_\backslash$. The explanation for the dynamical matching of these less "direct" trajectories to the conrotatory product is not obvious. This product is presumably preferred because the lighter bottom *perp*-CH_2 hydrogen can more effectively move and align with the methine and *tilt*-CH_2 hydrogens when they lie under the 3C plane. This effect increases the conrotatory force needed to rotate the 3C plane and the top *perp*-CH_2 deuterium into the *cis* allyl product geometry with the stable π electronic configuration. However, a significant minority of the trajectories escape to the disrotatory *trans* allyl product and appear no more or less direct than most of the conrotatory trajectories.

The d-substitution of the bottom hydrogen of the *perp*-CH_2 (*perp*-HCD) results in dynamics quite distinct from the *perp*-DCH top substitution, although the substitution again results in

DOI: 10.1021/acs.jpca.5b02834
J. Phys. Chem. A 2015, 119, 6611–6630

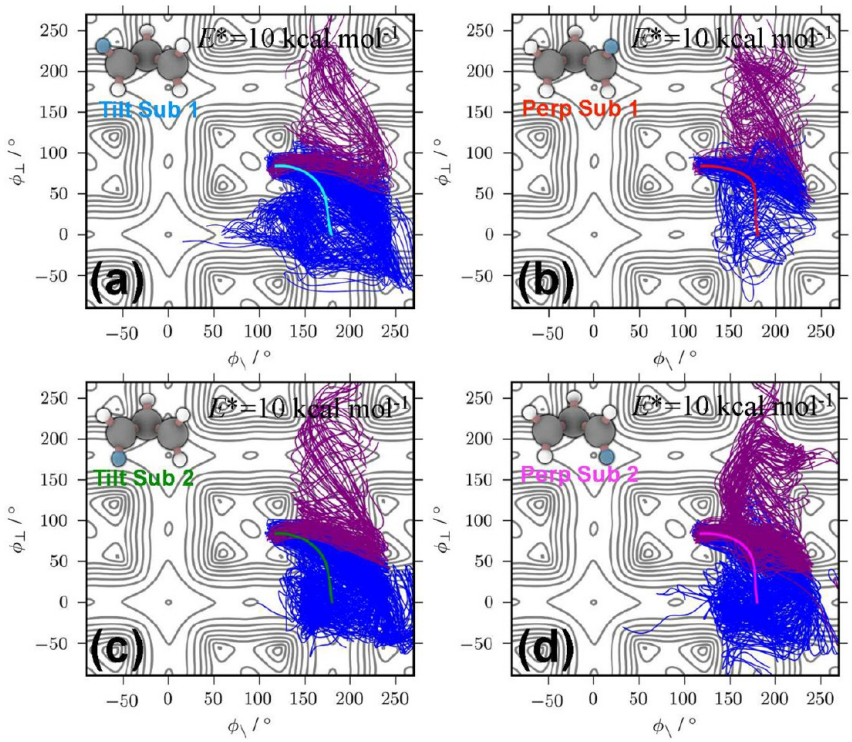

Figure 15. Full dimensional trajectories projected into the ($\phi_{\backslash}$, $\phi_{\perp}$) space for propagation times between 0 (the ring-opening TS crossing time) and 100 fs for the E^* = 10 kcal mol^{-1} ensemble for each of the four (a–d) CH_2 singly deuterated isotopomers of the cyclopropyl ring-opening TS.

important "local mode" motions of the *perp*-HCD hydrogen and deuterium. As seen in Figure 14d, the disrotatory bend is quite prominent for *perp*-HCD because the lighter top *perp*-HCD hydrogen motion is more easily induced as the ring opens than for the bottom deuterium. Trajectories can be divided into "direct" and "indirect" subsets. Direct trajectories proceed directly into the disrotatory *cis* allyl product region after the first $\phi_{\backslash}$ turning point, whereas indirect trajectories remain on the allyl ridge after the over-the-ridge collision event. All trajectories classified as conrotatory are indirect and all direct trajectories are classified as disrotatory. However, the division of the *perp*-HCD substitution trajectories into dis- and conrotatory mechanisms is more difficult and less distinct than in the previous cases, Table 2. Nevertheless, the disrotatory mechanism is favored due to the responsiveness of the top *perp*-HCD hydrogen to the disrotatory bend and *perp*-HCD wag.

For all four substitutions, the ring-opening IRCs were all disrotatory. However, the degree of synchrony of the IRC seems to roughly correlate with the dis- to conrotatory ratio in the E^* = 1 kcal mol^{-1} ensemble. Specifically, both *tilt*-CH_2 substitutions had IRCs that were more synchronous than the unsubstituted ring-opening, and the trajectories for both *tilt*-CH_2 substitutions were all disrotatory. The top *perp*-CH_2 substitutions had the least synchronous IRC and had the largest fraction of conrotatory trajectories. Lastly, the bottom *perp*-CH_2 substitution had an IRC similar to that of the unsubstituted reaction, and the dis- to conrotatory trajectory ratios for the two reactions were similar. This trend suggests the sensitivity of the IRC to mass substitution may be an indicator of a change in mechanism due to a Newtonian KIE (NKIE) even in cases were the reaction path symmetry does not exist; i.e., the IRC unambiguously connects at TS to one product isomer.

We have seen that the NKIE exists when the reaction is initiated at the ring-opening TS with a small amount of energy, E^* = 1 kcal mol^{-1}. However, the zero point energy of the ring-opening TS is ~40 kcal mol^{-1}, and therefore it is of interest to know if the NKIE persists for larger values of E^*. We show trajectory projections into the ($\phi_{\backslash}$, $\phi_{\perp}$) space for the four d-substitutions with E^* = 10 kcal mol^{-1} in Figure 15a–d, and the trajectory fractions are given in Table 2. As in the unsubstituted reaction, the dis- to conrotatory mechanism ratios of the d-substitution ring-openings become closer to one, but NKIE is still clearly present even though it is diminished.

Our results imply that the substitution of a hydrogen with a heavier atom such as a halogen may enhance the NKIE so that it persists at higher E^*, but at the expense of losing the symmetry of the PES. We have performed preliminary dynamics studies on the singly fluorine-substituted cyclopropyl ring-opening reaction and have found that this seems to be the case.

Our previous work on the 2d model PES[25] showed that the dynamics of reactions with reaction path bifurcations are sensitive to the shape of the potential. Displacing the location of one of the product minima dramatically changed product well occupancies over time. As Singleton and co-workers have pointed out,[58] a mass substitution is equivalent to a scaling of the potential in mass-weighted coordinates. The sensitivity of the mechanism of cyclopropyl radical ring-opening to deuterium substitution is analogous to the effect observed in the scaling of the generic 2d model PES.

Selectivity and Dynamics of the Allyl Product. Parts a and c of Figure 11 show that the allyl radical stereoisomer product can undergo CH_2 rotations subsequent to the ring-opening reaction. These rotations occur as the activated allyl products cross over the low energy allyl ridge between the allyl stereoisomer product regions. The selectivity of the ring-

DOI: 10.1021/acs.jpca.5b02834
J. Phys. Chem. A 2015, 119, 6611–6630

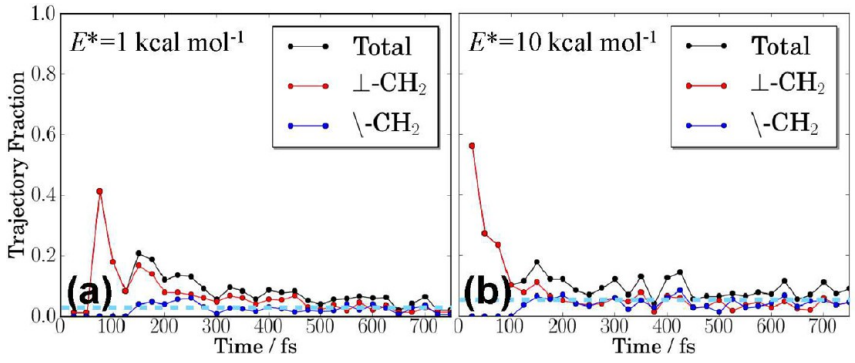

Figure 16. For (a) E^* = 1 kcal mol^{-1} and (b) E^* = 10 kcal mol^{-1}, the ensemble fraction of CH_2-group rotation events observed in an ensemble in 25 fs intervals is shown versus propagation time. The number of *perp*-CH_2 rotations is in red, the number of *tilt*-CH_2 rotations is in blue, and the sum of rotations of both CH_2 groups is in black. A rotation event is defined to occur whenever a ϕ angle passes through 90° or 270°. The classical RRKM prediction is shown as a dashed cyan line.

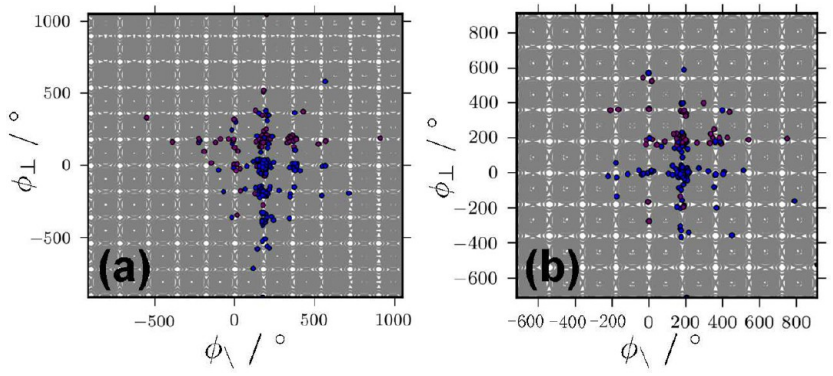

Figure 17. Trajectories projected into the ($\phi_\backslash$, $\phi_\perp$) space for the ring-opening reaction of cyclopropyl after 650 fs of propagation time for the (a) E^* = 1 and (b) E^* = 10 kcal mol^{-1} ensembles. The disrotatory (conrotatory) trajectories are shown in blue (purple).

opening reaction depends on whether there is some correlation between the initial ring-opening mechanism and a terminal, or at least long-lived, allyl stereoisomer. Simply put, the question of selectivity of the ring-opening reaction depends on the dynamics of the allyl radical product that follow the ring-opening.

The ring-opening reaction has only two possible allyl stereoisomer products corresponding to the outcome of the rotation of the *perp*-CH_2. However, there are four possible stereoisomers that can be reached by rotations of the *perp*-CH_2 and *tilt*-CH_2 groups of the allyl product. Parts a and b of Figure 16 show the number of CH_2-rotation events for each unsubstituted E^* ensemble, where a CH_2 group undergoes a rotation through a configuration where its plane is perpendicular to the 3C plane, observed in 25 fs time intervals versus propagation time. The high initial peaks correspond to the dynamics of the ring-opening process, but rotations of both the *perp*-CH_2 and *tilt*-CH_2 groups at later times are not uncommon. For reference, we have also computed the corresponding classical (harmonic) RRKM prediction for the number of CH_2-rotation events expected to occur in the allyl radical in a given 25 fs time scale, seen as a dashed line in Figure 16. The RRKM fraction represents the fraction of the classical microcanonical ensemble that undergoes a transition between allyl wells within a 25 fs time interval. Note that the RRKM prediction for the rate is similar to the actual dynamical rate at longer times, even though energy randomization within the ensemble is incomplete over the time interval shown. In either case, the allyl product produced by the ring-opening reaction is highly excited from the descent from the ∼60 kcal mol^{-1} barrier, and even if CH_2 rotation occurs statistically, abundant excitation energy makes the isomerization quite accessible. However, Figure 16 does clearly show that transitions between the allylic wells occur frequently and in both the E^* = 1 and 10 kcal mol^{-1} ensembles a majority of trajectories underwent at least one interallyl conversion after the initial ring-opening reaction during the simulation time. The trajectories in the unsubstituted ring-opening ensembles are shown in Figure 17a,b, where the spreading out of the trajectory ensemble among the possible allyl products over the propagation time is apparent.

In the deuterium substituted trajectories, particularly for the E^* = 1 kcal mol^{-1} ensembles, the post-ring-opening interallyl conversions due the rotation of the deuterated CH_2 group occurred more frequently and this effect was even more pronounced in our preliminary investigations of the fluorine substituted reaction. This is another aspect of the NKIE.

The allyl stereoisomer product population for the unsubstituted reaction ensembles are shown as a function of the propagation time in Figure 18a,b. It can be seen that the relative populations of the con- and disrotatory allyl products appear to stabilize at longer times ∼300 fs, but significant oscillations occur just following the ring-opening reaction. The contribution of direct disrotatory trajectories can be seen during the first ∼50−75 fs, with a sharp initial pulse due to the disrotatory bend and the choice of a large ϕ_{cutoff}. The conrotatory trajectories contribute to the allyl stereoisomer population at a later time than the direct disrotatory trajectories. At longer

DOI: 10.1021/acs.jpca.5b02834
J. Phys. Chem. A 2015, 119, 6611−6630

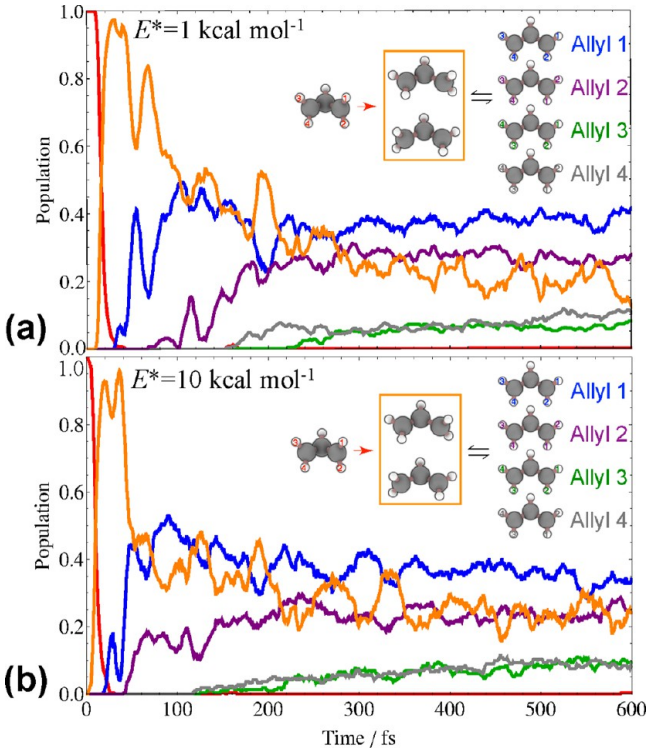

Figure 18. Allyl radical conformer product distributions as a function of propagation time. The red curve represents the trajectory fraction remaining near the transition state and the orange curve represents the fraction of trajectories in the "inter-allyl" region (where either of the CH_2 planes forms a dihedral angle with the 3C plane greater than 45°, but the α angle is still near the allyl product value). See Figure 7 for reference. In (a), the E^* = 1 kcal mol^{-1} ensemble is shown and in (b) the E^* = 10 kcal mol^{-1} is shown. Product stereoisomer distributions are determined with ϕ_{cutoff} = 45°, see text for details.

times for the E^* = 1 kcal mol^{-1} ensemble (Figure 18a), the disrotatory product has a slightly higher population than the conrotatory product and perhaps some relatively long-lasting disrotatory allyl preference occurs. However, a significant portion of the trajectories are not assigned to any product region at any time during the run and the general trend seems to be toward an equal distribution of the dis- and conrotatory products, allyls "1" and "2" in Figure 18. For the E^* = 10 kcal mol^{-1} ensemble, the dis- and conrotatory product populations are nearly equal by the end of 600 fs. Any nonstatistical product selectivity appears to have been eliminated in the post-ring-opening dynamics. The results do indicate that in both ensembles the formation of the indirect allyl products, allyls "3" and "4" in Figure 18, is much slower. Therefore, for nonstatistical product selectivity to occur in electrocyclic ring-opening systems, significant energy dissipation out of the important ring-opening degrees of freedom may be necessary on a time scale comparable to that of the initial reaction process. Such dissipation might arise from coupling to the solvent environment or from energy flow to other vibrational degrees of freedom within the product molecule that are not involved in isomerization. Such IVR is not substantial enough to affect product selectivity for ensembles studied here. However, solvent effects on the cyclopropyl ring-opening have been previously seen to have significant effect on the product selectivity.[28]

Dissipation. In the dynamics on the model 2d PES,[25] dissipation was included via the addition of a linear momentum frictional term to the equations of motion as in eq 1. A principal result of that work was the oscillation of the final product yield with variation of the dissipation factor γ, the inverse time scale of the dissipation, rather than a simple monotonic convergence to the statistical yield that might be expected as $\gamma \rightarrow 0$. This nonstatistical product yield oscillation as a function of dissipation strength raises the question whether such oscillations occur in more realistic VRI systems.

We have performed the same dissipation analysis as Collins et al. on the unsubstituted cyclopropyl ring-opening over a similar range of the magnitude of the dissipation parameter. Furthermore, the chosen range of γ encompasses interesting dynamical behavior of the cyclopropyl radical ring-opening under the frictional dissipation model and includes generally assumed energy relaxation time scales up to the order of picoseconds due to surrounding solvent or IVR. One E^* = 5 kcal mol^{-1} ensemble of 208 trajectories sampled at the ring-opening TS was propagated for several values of dissipation parameter, γ, chosen within an interval that corresponded to characteristic dissipation times between 10 fs and 5.7 ps. Trajectories were propagated until their energy was below the CH_2-rotation energetic barrier height, and they could be unambiguously assigned to an allyl stereoisomer product. The product yield versus dissipation parameter is shown in Figure 19. In Figures 20a–e, the ϕ space projections of the trajectories

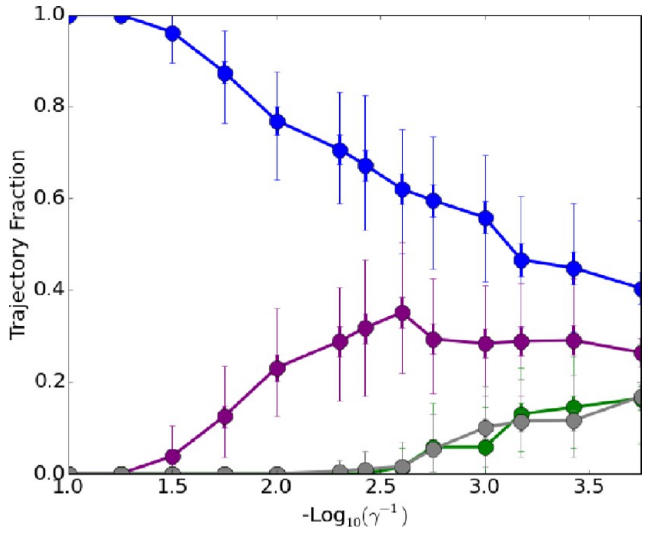

Figure 19. Product yield of a E^* = 5 kcal mol^{-1} ensemble of 208 ring-opening trajectories of the four stereoisomers of the allyl radical versus the negative logarithm of the dissipative parameter γ, eq 1a. Estimated error bars are also shown (thick bars are ±1 standard deviation, thin error bars are min and max error estimates, see Supporting Information). The color scheme is the same as Figure 7.

are shown along with corresponding time-resolved product populations in Figure 20A–E to give a sense of the reaction time scales. A description of the error bars in Figure 19 is given in the Supporting Information.

The model PES of Collins et al. differs from the cyclopropyl ring-opening in one key respect. The model PES is asymmetric across the surface dividing the two possible products, and the nonmonotonicity in the product yield was related critically to this PES asymmetry. In contrast, the PES in the ring-opening

DOI: 10.1021/acs.jpca.5b02834
J. Phys. Chem. A 2015, 119, 6611–6630

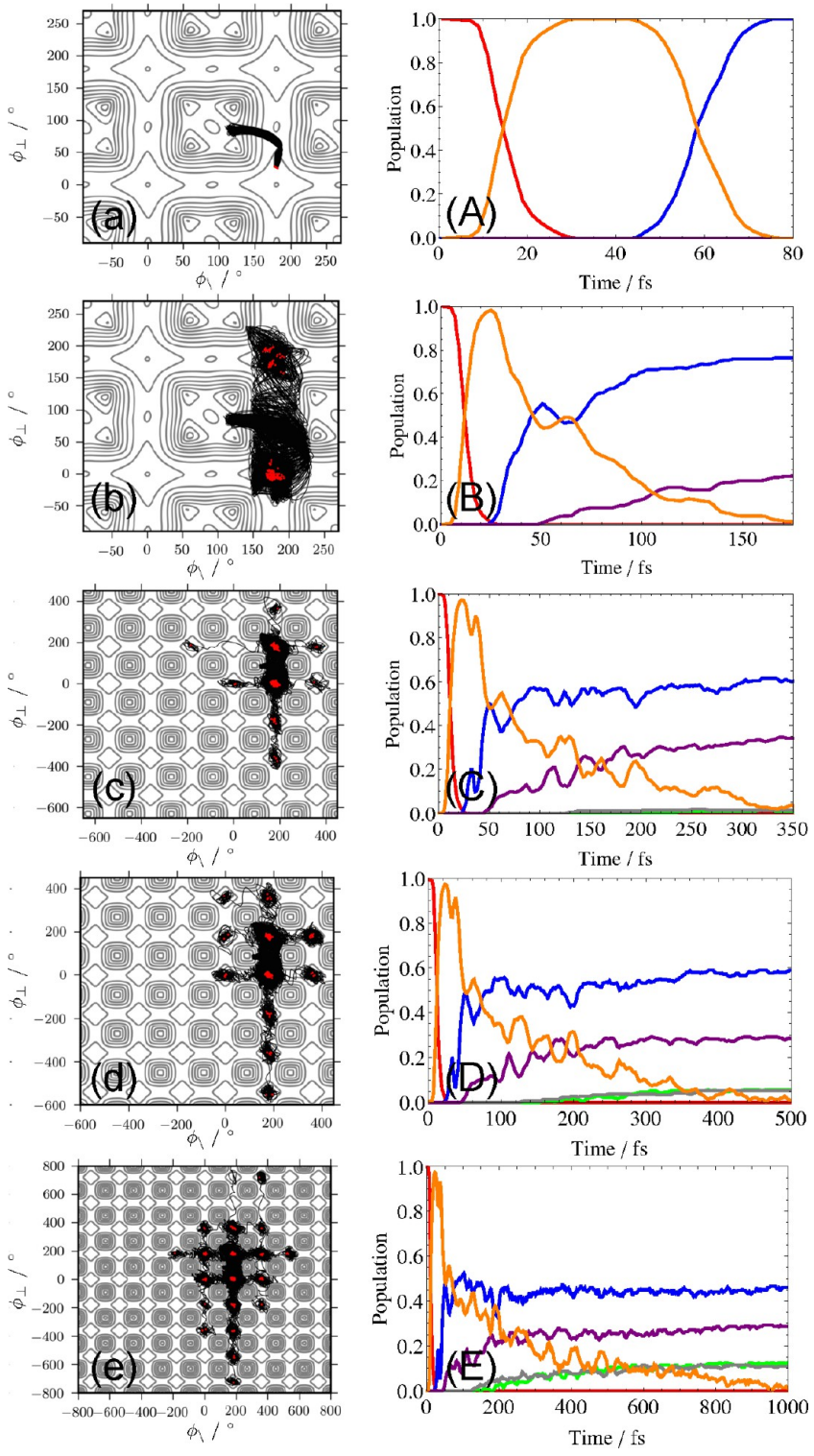

Figure 20. Trajectories of the dissipative ensembles (E^* = 5 kcal mol^{-1}) are shown projected in the ($\phi_\backslash$, $\phi_\perp$) space for several values of the dissipation parameter, γ = (a) 10^{-1} fs^{-1}, (b) 10^{-2} fs^{-1}, (c) $10^{-2.60}$ fs^{-1}, (d) $10^{-2.75}$ fs^{-1}, and (e) $10^{-3.18}$ fs^{-1}. End points of trajectories are shown as red dots. In (A)−(E), corresponding allyl stereoisomer product distributions are shown versus time. The color scheme is the same as in Figures 7 and 18. Product stereoisomer distributions are determined with ϕ_{cutoff} = 45°, see text for details.

reaction is symmetric about the surface dividing the allyl conformer product wells. As discussed above, asymmetry in the cyclopropyl reaction is introduced in the initial opening of the ring. Therefore, a nonmonotonicity effect in the allyl product yield analogous to that observed in the model PES must necessarily result solely from the allyl products' "dynamical memory" of the initial ring-opening, i.e., dynamical differences between the initial dis- or conrotatory mechanism.

Only the disrotatory allyl stereoisomer is produced in the presence of strong dissipation. In Figure 20a, γ^{-1} = 10 fs, the largest dissipation studied, the ensemble descends immediately into the disrotatory allyl stereoisomer well, similarly to the IRC.

DOI: 10.1021/acs.jpca.5b02834
J. Phys. Chem. A 2015, 119, 6611−6630

However, even with this very high dissipation a small departure from the IRC persists. No conrotatory product is observed until $\gamma^{-1} \approx 32$ fs ($\gamma = 10^{-1.5}$ fs^{-1}). The delayed appearance of the conrotatory stereoisomer is expected because conrotatory trajectories must travel farther along the allyl ridge to reach the conrotatory product well. For these trajectories, there is more time for the dissipation to act.

The contribution of the conrotatory product steadily grows between $\gamma^{-1} \approx 32$ and $\gamma^{-1} \approx 400$ fs (γ between $10^{-1.5}$ and $10^{-2.60}$ fs^{-1}) as the dissipation decreases sufficiently for that product channel to open. Save for a very small (2/208) fraction of trajectories, for $\gamma \leq 10^{-2.3}$ fs^{-1}, trajectories are observed to remain in the product region which they first enter; for example, see Figure 20b. For $\gamma > 10^{-2.3}$ fs^{-1}, a substantial number of subsequent rotations of the initially excited *perp*-CH_2 occur and multiple crossings between the con- and disrotatory allyl stereoisomers contribute to the product yield. The shapes of the trajectory paths in Figures 20a−e reveal that the excitation energy of the initially produced allyl is primarily localized in the $\phi_\perp$ motion. This is presumably the beginning of the manifestation of the same effect that gave an oscillatory product yield in the model system of Collins et al. analogous to "stereochemical scrambling" seen in several organic reactions.[74,75] However, the dramatic nonmonotonicity in the product yield of the model problem is not evident in Figure 19. It seems the dynamical memory of the trajectories is insufficient to maintain the coherent isomerization dynamics needed for significant oscillation of the product yield.

The most noticeable nonmonotonic feature of the product yield as a function of dissipation is the small decrease in the conrotatory allyl at $\gamma = 10^{-2.75}$ fs^{-1}. This corresponds to the fast rise in the other two allyl products, those not directly connected to the chosen ring-opening TS by a monotonic minimum energy dis- or conrotatory path. These unconnected allyl conformers appear in the product yield prior to $\gamma \sim 10^{-2.75}$ fs^{-1} but increase significantly only when $\gamma \geq 10^{-2.75}$ fs^{-1} ($\gamma^{-1} \sim 560$ fs); compare Figure 20c,d. The dissipation time scale of 560 fs is apparently long enough to allow significant energy transfer between the excited $\phi_\perp$ and $\phi_\backslash$ degrees of freedom. The small decrease in the conrotatory product yield at $\gamma = 10^{-2.75}$ fs^{-1} does not appear to recover at smaller dissipation. The slight decrease in the conrotatory product curve is due to the appreciable opening of the unconnected allyl product channels via rotation of the *tilt*-CH_2 group.

Whether any significant oscillations in the product yield appear for smaller values of γ was not explored as the propagation times required for such calculations were prohibitively long. For the smallest dissipations studied ($\gamma^{-1} \approx 5.6$ ps), the product yield appears to be approaching its statistical limit, where all the possible allyl stereoisomers contribute equally. Nevertheless, the delayed appearance of the conrotatory product followed by the subsequent distinct rise of the unconnected allyl isomer products illustrates how varying environmental dissipation (e.g., changing solvent or substituting different nonreactive functional groups on a reactant, and tuning the dissipation time scale relative to the stereochemical isomerization time scale) can be used to modulate product selectivity. In closing, we note that our simple treatment of dissipation for the cyclopropyl problem is consistent with the results of Halls and Mann[28] who studied the cyclopropyl radical ring-opening in more realistic Ar and He bath environments.

CONCLUSION

In this work, we have studied the post-transition state (TS) dynamics of the ring-opening of the cyclopropyl radical to form the allyl radical, a reaction known to have a reaction path bifurcation into paths involving dis- and conrotatory rotations of the methylenes. The intrinsic reaction coordinate (IRC) for the reaction was disrotatory and corresponded to relatively asynchronous rotations, first of the CH_2 group that was already significantly rotated at the ring-opening TS (*tilt*-CH_2), followed by rotation of the CH_2 group almost orthogonal to the carbon plane at the ring-opening TS, the *perp*-CH_2. The IRC remains disrotatory for all possible single deuterium substitutions of the methylene hydrogens. However, the deuterium substitutions were found to change the degree of synchrony in the rotations of the methylenes along the IRC. Substitutions on the *tilt*-CH_2 led to a more pronounced synchronous character, whereas top substitution (that of the methylene hydrogen on the same side of the carbon plane as the methine hydrogen) on the *perp*-CH_2 emphasized asynchronous character. These shifts in the character of the IRC coincide with a significant shift of the mechanism manifested within the dynamics. Calculations of a reduced dimensional potential energy surface (PES) in a subset of key coordinates (the allyl carbon backbone bond angle, α, and the two methylene dihedrals relative to the carbon plane, $\phi_\backslash$ and $\phi_\perp$) reveal that the reaction occurs by passage from the ring-opening transition state dividing surface onto a lower energy ridge. This ridge corresponds to the *tilt*-CH_2 lying in the carbon plane, while the *perp*-CH_2 remains perpendicular to the carbon plane. Traversal of the ridge involves passage between allyl conformers by the rotation of the *perp*-CH_2.

Propagation of trajectories from the ring-opening TS toward the allyl product for microcanonical ensembles sampled at excitation energies $E^* = 1$ and 10 kcal mol^{-1} above the ring-opening saddle point reveals that the disrotatory mechanism is dominant, but the conrotatory mechanism contributes significantly, in agreement with previous studies.[27,28]

We observe that the mechanism-deciding step in the dynamics occurs in a "collision" event analogous to that seen in previous work on a 2d model PES.[25] This event corresponds to passage over the ridge structure in the PES to a highly distorted configuration space of the allyl with the *perp*-CH_2 remaining out of the carbon plane. When the "hard wall" of the potential is reached, trajectories that have not already followed the disrotatory route are significantly dispersed in the $\phi_\perp$ coordinate, with those trajectories with high $\phi_\perp$ mostly heading to the conrotatory well and those with a low value of $\phi_\perp$ heading to the disrotatory well. Several large amplitude motions of the floppy allyl molecule, such as the wag of *perp*-CH_2 and the "local mode" bending of the *perp*-CH_2 hydrogens, were seen to be important to the dynamics.

An interesting Newtonian kinetic isotope effect was observed in the dynamics upon the deuterium substitution of the methylene hydrogens. Substitutions of the *tilt*-CH_2 group caused the dynamics to favor the disrotatory mechanism. Substitution of the top *perp*-CH_2 hydrogen resulted in a strong preference for the conrotatory mechanism. This mass effect was consistent with our previous work on a 2d model potential, where the product ratio and dynamics were found to be quite sensitive to even very slight scalings of the potential, analogous to mass substitution in the present case. The direction of the shift in the mechanism also correlated with the nature of the shift of the IRC to either more synchronous or more

DOI: 10.1021/acs.jpca.5b02834
J. Phys. Chem. A 2015, 119, 6611−6630

asynchronous character by the deuterium substitution, with the former preferring the disrotatory mechanism and the latter preferring the conrotatory mechanism. Although sensitivity of the character of the IRC to isotopic substitution is an indicator of the presence of a Newtonian kinetic isotope effect (NKIE), our observations reveal additional dynamical aspects of the NKIE.

To model environmental effects, a dissipative friction force was added to the equations of motion for an $E^* = 5$ kcal mol^{-1} trajectory ensemble. This ensemble was propagated until sufficient energy had dissipated to unambiguously assign an allyl radical conformer product well to each trajectory. The pronounced oscillations of the product yield as a function of the dissipation parameter observed in the 2d model potential were not observed for the cyclopropyl ring-opening. Such oscillations are most likely to appear in systems where the key reaction motions are weakly coupled to the other intramolecular degrees of freedom, and in PESs with less symmetry than observed in the allyl radical isomerization process. The dissipation work highlights the possibility of using environmental factors (e.g., solvent and pressure) to control the product selectivity in similar electrocyclic reactions. Such control is based on the competing time scales of dissipation and product isomerization.

In summary, the ring-opening of the cyclopropyl radical has shown many dynamical similarities to the 2d model potential previously studied. Such models can give much insight into reactions with inherently multidimensional reaction coordinates and can be valuable tools in mechanistic organic chemistry. Indeed, although direct dynamics simulations of complex organic systems are of great utility and are becoming quite common, the interpretation of the results of such simulations can be both challenging and ambiguous. Lower dimensional models can be effectively characterized and visualized, and the dynamics of such models can be efficiently explored in great detail. Nevertheless, the cyclopropyl ring-opening does contain some features that are not fully captured by the low dimensional models. Chemical reactions involving reaction path bifurcations often feature an intermediate with a "floppy" moiety with several possible large amplitude motions. In the case where large amplitude spectator motions are sufficiently excited after passing through a high energy barrier, the observed dynamics can be more complicated than is seen in a reduced dimensional model.

■ ASSOCIATED CONTENT

Supporting Information

Equilibrium geometries and vibrational frequencies of stationary points on the potential energy surface of the cyclopropyl ring-opening reaction, various contour plots of the reduced dimensional potential energy surface in $(\phi_\backslash, \phi_\perp)$ space, and results of the preliminary $T = 447$ K ensemble. The Supporting Information is available free of charge on the ACS Publications website at DOI: 10.1021/acs.jpca.5b02834.

■ AUTHOR INFORMATION

Corresponding Authors

*Z. C. Kramer. E-mail: zck3@cornell.edu.
*B. K. Carpenter. E-mail: CarpenterB1@cardiff.ac.uk.
*G. S. Ezra. E-mail: gse1@cornell.edu.
*S. Wiggins. E-mail: stephen.wiggins@mac.com.

Notes

The authors declare no competing financial interest.

■ ACKNOWLEDGMENTS

The work of Z.C.K. and G.S.E. is supported by the US National Science Foundation under Grant No. CHE-1223754. Z.C.K. thanks Dr. Toby Zeng for helpful discussions. B.K.C. and S.W. acknowledge the support of the UK Engineering and Physical Sciences Research Council (Grant No. EP/K000489/1). S.W. acknowledges the support of the Office of Naval Research (Grant No. N00014-01-0769). This work was carried out using the computational resources of the Advanced Computing Research Centre, University of Bristol - http://www.bris.ac.uk/acrc/.

■ REFERENCES

(1) Woodward, R. B.; Hoffmann, R. The conservation of orbital symmetry. *Angew. Chem., Int. Ed. Engl.* **1969**, *8*, 781−853.
(2) Woodward, R. B.; Hoffmann, R. Stereochemistry of electrocyclic reactions. *J. Am. Chem. Soc.* **1965**, *87*, 395−397.
(3) Longuet-Higgins, H. C.; Abrahamson, E. W. The electronic mechanism of electrocyclic reactions. *J. Am. Chem. Soc.* **1965**, *87*, 2045−2046.
(4) Boche, G.; Szeimies, G. Electrocyclic reactions of radicals. *Angew. Chem., Int. Ed. Engl.* **1971**, *10*, 911−912.
(5) Greig, G.; Thynne, J. C. J. Reactions of cyclic alkyl radicals. Part 1.-Methyl-radical-sensitized decomposition of cyclopropane carboxyldehyde. *Trans. Faraday Soc.* **1966**, *62*, 3338−3344.
(6) Greig, G.; Thynne, J. C. J. Reactions of cyclic alkyl radicals. Part 2.-Photolysis of cyclopropane carboxaldehyde. *Trans. Faraday Soc.* **1967**, *63*, 1369−1374.
(7) Walsh, R. Cyclic alkyl radical isomerization: A correction to the literature. *Int. J. Chem. Kinet.* **1970**, *2*, 71−74.
(8) Dewar, M. J. S.; Kirschner, S. Nature of the transition states in forbidden electrocyclic reactions. *J. Am. Chem. Soc.* **1974**, *96*, 5244−5246.
(9) Arnold, P. A.; Carpenter, B. K. Computational studies on the ring-openings of cyclopropyl radical and cyclopropyl cation. *Chem. Phys. Lett.* **2000**, *328*, 90−96.
(10) Olivella, S.; Sole, A.; Bofill, J. M. A theoretical investigation of the thermal ring-opening of cyclopropyl radical into allyl radical. Evidence for a highly nonsymmetric transition state. *J. Am. Chem. Soc.* **1990**, *112*, 2160−2167.
(11) Liu, K.; Zhao, H.-M.; Ma, S.-Y.; Li, Z.-H. Computational study of the thermal ring-opening of cyclopropyl radical, cation and anion. *J. Mol. Struct.: THEOCHEM* **2004**, *672*, 209−213.
(12) Chen, C.; Braams, B.; Lee, D. Y.; Bowman, J. M.; Houston, P. L.; Stranges, D. The dynamics of allyl radical dissociation. *J. Phys. Chem. A* **2011**, *115*, 6797−6804.
(13) Castiglioni, L.; Bach, A.; Chen, P. Spectroscopy and dynamics of A $[^2B_1]$ allyl radical. *Phys. Chem. Chem. Phys.* **2006**, *8*, 2591−2598.
(14) Fukui, K. The path of chemical reactionsthe IRC approach. *Acc. Chem. Res.* **1981**, *14*, 363−368.
(15) Quapp, W.; Bofill, J. Topography of cyclopropyl radical ring-opening to allyl radical on the CASSCF(3,3) surface: valley-ridge inflection points by Newton trajectories. *J. Math. Chem.* **2012**, *50*, 2061−2085.
(16) Quapp, W.; Bofill, J. M.; AguilarMogas, A. Exploration of cyclopropyl radical ring-opening to allyl radical by Newton trajectories: Importance of valley-ridge inflection points to understand the topography. *Theor. Chem. Acc.* **2011**, *129*, 803−821.
(17) Quapp, W.; Heidrich, D. Analysis of the concept of minimum energy path on the potential energy surface of chemically reacting systems. *Theor. Chim. Acta.* **1984**, *66*, 245−260.
(18) Quapp, W.; Hirsch, M.; Heidrich, D. Bifurcation of reaction pathways: The set of valley ridge inflection points of a simple three-

DOI: 10.1021/acs.jpca.5b02834
J. Phys. Chem. A 2015, 119, 6611−6630

dimensional potential energy surface. *Theor. Chem. Acc.* **1998**, *100*, 285−299.
(19) Quapp, W. How does a reaction path branching take place? A classification of bifurcation events. *J. Mol. Struct.* **2004**, *695*, 95−101.
(20) Sugny, D.; Kontz, C.; Ndong, M.; Justum, Y.; Dive, G.; Desouter-Lecomte, M. Laser control in a bifurcating region. *Phys. Rev. A: At., Mol., Opt. Phys.* **2006**, *74*, 043419.
(21) Lasorne, B.; Dive, G.; Desouter-Lecomte, M. Wave packets in a bifurcating region of an energy landscape: Diels-Alder dimerization of cyclopentadiene. *J. Chem. Phys.* **2005**, *122*, 184304.
(22) Taketsugu, T.; Tajima, N.; Hirao, K. Approaches to bifurcating reaction path. *J. Chem. Phys.* **1996**, *105*, 1933−1939.
(23) Metiu, H.; Ross, J.; Silbey, R.; George, T. F. On symmetry properties of reaction coordinates. *J. Chem. Phys.* **1974**, *61*, 3200−3209.
(24) Valtazanos, P.; Ruedenberg, K. Bifurcations and transition states. *Theor. Chem. Acta* **1986**, *69*, 281−307.
(25) Collins, P.; Carpenter, B. K.; Ezra, G. S.; Wiggins, S. Nonstatistical dynamics on potentials exhibiting reaction path bifurcations and valley-ridge inflection points. *J. Chem. Phys.* **2013**, *139*, 154108.
(26) Carpenter, B. K. Energy disposition in reactive intermediates. *Chem. Rev.* **2013**, *113*, 7265−7286.
(27) Mann, D. J.; Hase, W. L. Ab initio direct dynamics study of cyclopropyl radical ring-opening. *J. Am. Chem. Soc.* **2002**, *124*, 3208−3209.
(28) Mann, D. J.; Halls, M. D. Ring-opening of the cyclopropyl radical in the condensed phase: A combined density functional theory/molecular mechanics quasiclassical trajectory study. *Phys. Chem. Chem. Phys.* **2002**, *4*, 5066−5071.
(29) Carpenter, B. K. Nonstatistical dynamics in thermal reactions of polyatomic molecules. *Annu. Rev. Phys. Chem.* **2005**, *56*, 57−89.
(30) Yamataka, H. Molecular dynamics simulations and mechanism of organic reactions: NonTST behaviors. *Adv. Phys. Org. Chem.* **2010**, *44*, 173−222.
(31) Bachrach, S. *Computational Organic Chemistry*; Wiley: New York, 2007.
(32) Bogle, X. S.; Singleton, D. A. Dynamic origin of the stereoselectivity of a nucleophilic substitution reaction. *Org. Lett.* **2012**, *14*, 2528−2531.
(33) Oyola, Y.; Singleton, D. A. Dynamics and the failure of transition state theory in alkene hydroboration. *J. Am. Chem. Soc.* **2009**, *131*, 3130−3131.
(34) Birney, D. Theory, experiment and unusual features of potential energy surfaces of pericyclic and pseudopericyclic reactions with sequential transition structures. *Curr. Org. Chem.* **2010**, *14*, 1658−1668.
(35) Ess, D.; Wheeler, S.; Iafe, R.; Xu, L.; Çelebi-Ölçüm, N.; Houk, K. Bifurcations on potential energy surfaces of organic reactions. *Angew. Chem., Int. Ed.* **2008**, *47*, 7592−7601.
(36) Zheng, J.; Papajak, E.; Truhlar, D. G. Phase space prediction of product branching ratios: Canonical competitive nonstatistical model. *J. Am. Chem. Soc.* **2009**, *131*, 15754−15760.
(37) Carpenter, B. K. Taking the high road and getting there before you. *Science* **2011**, *332*, 1269−1270.
(38) Rehbein, J.; Carpenter, B. K. Do we fully understand what controls chemical selectivity? *Phys. Chem. Chem. Phys.* **2011**, *13*, 20906−20922.
(39) Carpenter, B. K. Intramolecular dynamics for the organic chemist. *Acc. Chem. Res.* **1992**, *25*, 520−528.
(40) Hong, Y. J.; Tantillo, D. J. Biosynthetic consequences of multiple sequential post-transition-state bifurcations. *Nat. Chem.* **2014**, *6*, 104−111.
(41) Mauguiére, F. A. L.; Collins, P.; Ezra, G. S.; Farantos, S. C.; Wiggins, S. Roaming dynamics in ion−molecule reactions: Phase space reaction pathways and geometrical interpretation. *J. Chem. Phys.* **2014**, *140*, 134112.
(42) Mauguiére, F. A. L.; Collins, P.; Ezra, G. S.; Farantos, S. C.; Wiggins, S. Multiple transition states and roaming in ionmolecule reactions: A phase space perspective. *Chem. Phys. Lett.* **2014**, *592*, 282−287.
(43) DeFrees, D. J.; McIver, R. T.; Hehre, W. J. Heats of formation of gaseous free radicals via ion cyclotron double resonance spectroscopy. *J. Am. Chem. Soc.* **1980**, *102*, 3334−3338.
(44) Lu, D.; Hase, W. L. Classical mechanics of intramolecular vibrational energy flow in benzene. V. Effect of zeropoint energy motion. *J. Chem. Phys.* **1989**, *91*, 7490−7497.
(45) Aquilante, F.; Jensen, K. P.; Roos, B. O. The allyl radical revisited: A theoretical study of the electronic spectrum. *Chem. Phys. Lett.* **2003**, *380*, 689−698.
(46) Yamaguchi, M. A. CASSCF study of photochemical cyclization of the first excited $\tilde{A}\ ^2B_1$ state of the allyl radical. *J. Mol. Struct.: THEOCHEM* **1996**, *365*, 143−149.
(47) The conical intersections are found using SA-CASSCF(3,3)/6-31+G(d,p). The VRI point structure is taken from Quapp et al.[15] and the energy calculated at CASSCF(3,3)/6-31+G(d,p).
(48) Schmidt, M. W.; Baldridge, K. K.; Boatz, J. A.; Elbert, S. T.; Gordon, M. S.; Jensen, J. H.; Koseki, S.; Matsunaga, N.; Nguyen, K. A.; Su, S.; et al. General atomic and molecular electronic structure system. *J. Comput. Chem.* **1993**, *14*, 1347−1363.
(49) Gordon, M. S.; Schmidt, M. In *Theory and applications of Computational Chemistry: the first forty years*; Dykstra, C., Frenking, G., Kim, K., Scuserica, G., Eds.; Elsevier: Amsterdam, 2005; pp 1167−1189.
(50) Korth, H.-G.; Trill, H.; Sustmann, R. [1−2H]-Allyl radical: barrier to rotation and allyl delocalization energy. *J. Am. Chem. Soc.* **1981**, *103*, 4483−4489.
(51) Conte, R.; Houston, P. L.; Bowman, J. M. Classical trajectory study of energy transfer in collisions of highly excited allyl radical with argon. *J. Phys. Chem. A* **2013**, *117*, 14028−14041.
(52) Jean, Y.; Chapuisat, X. Dynamical study of mechanistic details in organic reactions. I. Two-step study of isomerizations of cyclopropane-type molecules. *J. Am. Chem. Soc.* **1974**, *96*, 6911−6920.
(53) Chapuisat, X.; Jean, Y. Dynamical study of mechanistic details in organic reactions. II. Overall study of isomerizations of cyclopropane. *J. Am. Chem. Soc.* **1975**, *97*, 6325−6337.
(54) M. Goldfield, E. Quantum dynamics of the trimethylene biradical Stereomutation of cyclopropane and unimolecular decay. *Faraday Discuss.* **1998**, *110*, 185−205.
(55) Valtazanos, P.; Elbert, S.; Xantheas, S.; Ruedenberg, K. The ring-opening of cyclopropylidene to allene: global features of the reaction surface. *Theor. Chim. Acta* **1991**, *78*, 287−326.
(56) Wilson, E.; Decius, J.; Cross, P. *Molecular Vibrations: The Theory of Infrared and Raman Vibrational Spectra*; Dover Books on Chemistry Series; Dover Publications: New York, 1955.
(57) Doubleday, C.; Suhrada, C. P.; Houk, K. N. Dynamics of the degenerate rearrangement of bicyclo[3.1.0]hex-2-ene. *J. Am. Chem. Soc.* **2006**, *128*, 90−94.
(58) Singleton, D. A.; Hang, C.; Szymanski, M. J.; Greenwald, E. E. A new form of kinetic isotope effect. Dynamic effects on isotopic selectivity and regioselectivity. *J. Am. Chem. Soc.* **2003**, *125*, 1176−1177.
(59) Bunker, D. L.; Hase, W. L. On non - RRKM unimolecular kinetics: Molecules in general, and CH_3NC in particular. *J. Chem. Phys.* **1973**, *59*, 4621−4632.
(60) Hase, W. L.; Duchovic, R. J.; Hu, X.; Komornicki, A.; Lim, K. F.; Lu, D.-h.; Peslherbe, G. H.; Swamy, K. N.; Vande Linde, S. R.; Varandas, A. VENUS96: A general chemical dynamics computer program.*QCPE Bull.* **1996**, *16*, available at http://works.bepress.com/ronald_duchovic/9.
(61) Hase, W. L.; Ludlow, D. M.; Wolf, R. J.; Schlick, T. Translational and vibrational energy dependence of the cross section for $H + C_2H_4 \rightarrow C_2H_5^*$. *J. Phys. Chem.* **1981**, *85*, 958−968.
(62) Hu, X.; Hase, W. L.; Pirraglia, T. Vectorization of the general Monte Carlo classical trajectory program VENUS. *J. Comput. Chem.* **1991**, *12*, 1014−1024.
(63) Swope, W. C.; Andersen, H. C.; Berens, P. H.; Wilson, K. R. A computer simulation method for the calculation of equilibrium

DOI: 10.1021/acs.jpca.5b02834
J. Phys. Chem. A 2015, 119, 6611−6630

constants for the formation of physical clusters of molecules: Application to small water clusters. *J. Chem. Phys.* **1982**, *76*, 637−649.
(64) Taketsugu, T.; Gordon, M. S. Dynamic reaction coordinate analysis: An application to $SiH_4 + H^- \rightarrow SiH_5^-$. *J. Phys. Chem.* **1995**, *99*, 8462−8471.
(65) Sun, L.; Hase, W. L. Comparisons of classical and Wigner sampling of transition state energy levels for quasiclassical trajectory chemical dynamics simulations. *J. Chem. Phys.* **2010**, *133*, 044313.
(66) Hase, W. L.; Buckowski, D. G. Monte carlo sampling of a microcanonical ensemble of classical harmonic oscillators. *Chem. Phys. Lett.* **1980**, *74*, 284−287.
(67) Besold, G.; Vattulainen, I.; Karttunen, M.; Polson, J. M. Towards better integrators for dissipative particle dynamics simulations. *Phys. Rev. E: Stat. Phys., Plasmas, Fluids, Relat. Interdiscip. Top.* **2000**, *62*, R7611−R7614.
(68) Gonzalez, C.; Schlegel, H. B. An improved algorithm for reaction path following. *J. Chem. Phys.* **1989**, *90*, 2154−2161.
(69) Tarini, M.; Cignoni, P.; Montani, C. Ambient occlusion and edge cueing for enhancing real time molecular visualization. *IEEE Trans. Visualization and Computer Graphics* **2006**, *12*, 1237−1244.
(70) Collins, P.; Kramer, Z. C.; Carpenter, B. K.; Ezra, G. S.; Wiggins, S. Nonstatistical dynamics on the caldera. *J. Chem. Phys.* **2014**, *141*, 034111.
(71) Takahashi, K.; Kramer, Z. C.; Vaida, V.; Skodje, R. T. Vibrational overtone induced elimination reactions within hydrogenbonded molecular clusters: The dynamics of water catalyzed reactions in $CH_2FOH(H_2O)_n$. *Phys. Chem. Chem. Phys.* **2007**, *9*, 3864−3871.
(72) Andujar-de Sanctis, I. L.; Singleton, D. A. Racing carbon atoms. Atomic motion reaction coordinates and structural effects on newtonian kinetic isotope effects. *Org. Lett.* **2012**, *14*, 5238−5241.
(73) Kelly, K. K.; Hirschi, J. S.; Singleton, D. A. Newtonian kinetic isotope effects. Observation, prediction, and origin of heavyatom dynamic isotope effects. *J. Am. Chem. Soc.* **2009**, *131*, 8382−8383.
(74) Glowacki, D. R.; Marsden, S. P.; Pilling, M. J. Significance of nonstatistical dynamics in organic reaction mechanisms: Time-dependent stereoselectivity in cyclopentynealkene cycloadditions. *J. Am. Chem. Soc.* **2009**, *131*, 13896−13897.
(75) Goldman, L. M.; Glowacki, D. R.; Carpenter, B. K. Nonstatistical dynamics in unlikely places: [1,5] hydrogen migration in chemically activated cyclopentadiene. *J. Am. Chem. Soc.* **2011**, *133*, 5312−5318.

DOI: 10.1021/acs.jpca.5b02834
J. Phys. Chem. A 2015, 119, 6611−6630